Resource

Cell Reports

Genetic Investigation of Tricarboxylic Acid Metabolism during the *Plasmodium falciparum* Life Cycle

Graphical Abstract

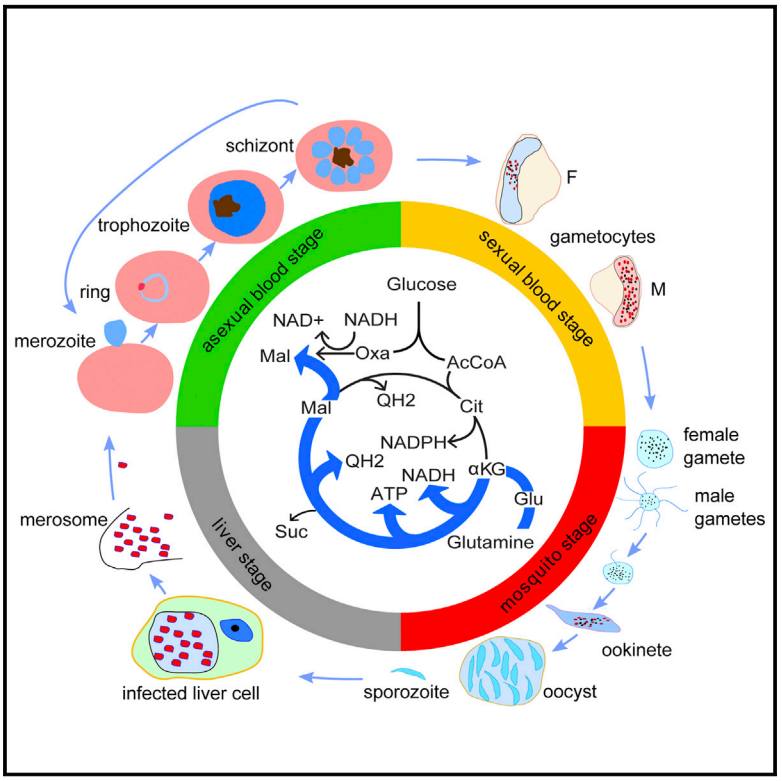

Highlights

- Six of the eight TCA cycle enzymes were knocked out without affecting asexual growth
- Metabolic labeling was analyzed in nine TCA KOs via ^{13}C-labeling and mass spectrometry
- The TCA cycle is adaptable, and the effect of a disrupted TCA cycle is stage specific

Authors

Hangjun Ke, Ian A. Lewis, ..., Manuel Llinás, Akhil B. Vaidya

Correspondence

avaidya@drexelmed.edu

In Brief

Mitochondria of malaria parasites have features that are divergent from their host's mitochondria. Ke et al. show that six of the TCA cycle enzymes can be disrupted without affecting asexual stages of *Plasmodium falciparum*. The TCA cycle is adaptable and is essential in insect stages of the parasite.

Accession Numbers

GSE59015

Ke et al., 2015, Cell Reports *11*, 164–174
April 7, 2015
http://dx.doi.org/10.1016/j.celrep.2015.03.011

OPEN ACCESS
CellPress

Cell Reports
Resource

Genetic Investigation of Tricarboxylic Acid Metabolism during the *Plasmodium falciparum* Life Cycle

Hangjun Ke,[1,5] Ian A. Lewis,[2,5,7] Joanne M. Morrisey,[1] Kyle J. McLean,[3] Suresh M. Ganesan,[1,6] Heather J. Painter,[2,8] Michael W. Mather,[1] Marcelo Jacobs-Lorena,[3] Manuel Llinás,[2,4,8] and Akhil B. Vaidya[1,*]

[1]Center for Molecular Parasitology, Drexel University College of Medicine, Philadelphia, PA 19129, USA
[2]Lewis-Sigler Institute for Integrative Genomics, Princeton University, Princeton, NJ 08544, USA
[3]Department of Molecular Microbiology and Immunology, Johns Hopkins School of Public Health, Baltimore, MD 21205, USA
[4]Department of Molecular Biology, Princeton University, Princeton, NJ 08544, USA
[5]Co-first author
[6]Present address: Department of Biological Engineering, Massachusetts Institute of Technology, Cambridge, MA 02139, USA
[7]Present address: Department of Biological Sciences, University of Calgary, Calgary, AB T2N 1N4, Canada
[8]Present address: Department of Biochemistry and Molecular Biology and Center for Malaria Research, Penn State University, State College, PA 16802, USA
*Correspondence: avaidya@drexelmed.edu
http://dx.doi.org/10.1016/j.celrep.2015.03.011

SUMMARY

New antimalarial drugs are urgently needed to control drug-resistant forms of the malaria parasite *Plasmodium falciparum*. Mitochondrial electron transport is the target of both existing and new antimalarials. Herein, we describe 11 genetic knockout (KO) lines that delete six of the eight mitochondrial tricarboxylic acid (TCA) cycle enzymes. Although all TCA KOs grew normally in asexual blood stages, these metabolic deficiencies halted life-cycle progression in later stages. Specifically, aconitase KO parasites arrested as late gametocytes, whereas α-ketoglutarate-dehydrogenase-deficient parasites failed to develop oocysts in the mosquitoes. Mass spectrometry analysis of ^{13}C-isotope-labeled TCA mutant parasites showed that *P. falciparum* has significant flexibility in TCA metabolism. This flexibility manifested itself through changes in pathway fluxes and through altered exchange of substrates between cytosolic and mitochondrial pools. Our findings suggest that mitochondrial metabolic plasticity is essential for parasite development.

INTRODUCTION

Malaria is a major global parasitic disease that is responsible for ~300 million infections and ~600,000 deaths per year (WHO, 2013). Although there are a number of effective antimalarial drugs available, the continued emergence of drug-resistant parasites (Ariey et al., 2014) has made finding new treatments a global health priority. Some existing drugs and promising lead compounds target the parasite's mitochondrial functions (Fry and Pudney, 1992; Nilsen et al., 2013; Phillips et al., 2008). The parasite's mitochondrion is highly divergent from its human counterpart (Vaidya and Mather, 2009), which provides a basis for selective toxicity of antimalarial drugs. However, the tricarboxylic acid (TCA) cycle, a fundamental metabolic pathway within the parasite mitochondrion, has not been fully explored as a potential drug target.

Several lines of evidence support the existence of TCA reactions in the human malaria parasite, *Plasmodium falciparum.* The parasite's genome encodes all of the TCA cycle enzymes (Gardner et al., 2002), which are expressed during the asexual stages (Bozdech et al., 2003). The eight TCA enzymes have been localized to the mitochondrion (Günther et al., 2005; Hodges et al., 2005; Takeo et al., 2000; Tonkin et al., 2004; H.K., J.M.M., M.W.M., and A.B.V., unpublished data), and TCA cycle intermediates are actively synthesized (Olszewski et al., 2009). More recently, isotopic labeling studies have demonstrated an active canonical oxidative TCA cycle. Glutamine and glucose are the main carbon sources for the TCA reactions in *P. falciparum* (Cobbold et al., 2013; MacRae et al., 2013). Glutamine carbon enters the cycle via α-ketoglutarate, whereas glucose appears to provide acetyl-CoA (Cobbold et al., 2013; MacRae et al., 2013), as well as some oxaloacetate (Storm et al., 2014), for entry at the citrate synthase (CS) step. The mitochondrial acetyl-CoA is produced from pyruvate by a branched-chain keto acid dehydrogenase (BCKDH) (Oppenheim et al., 2014).

Although recent studies have investigated metabolic flow through the TCA cycle in *Plasmodium* parasites (Cobbold et al., 2013; MacRae et al., 2013; Oppenheim et al., 2014; Storm et al., 2014), a broad analysis of TCA metabolism using genetic disruptions in *P. falciparum* has not been conducted until now. Previously, succinate dehydrogenase (*SDH*) was knocked out in the rodent parasite *P. berghei* (Hino et al., 2012), and knocked down in the human parasite *P. falciparum* (Tanaka et al., 2012),

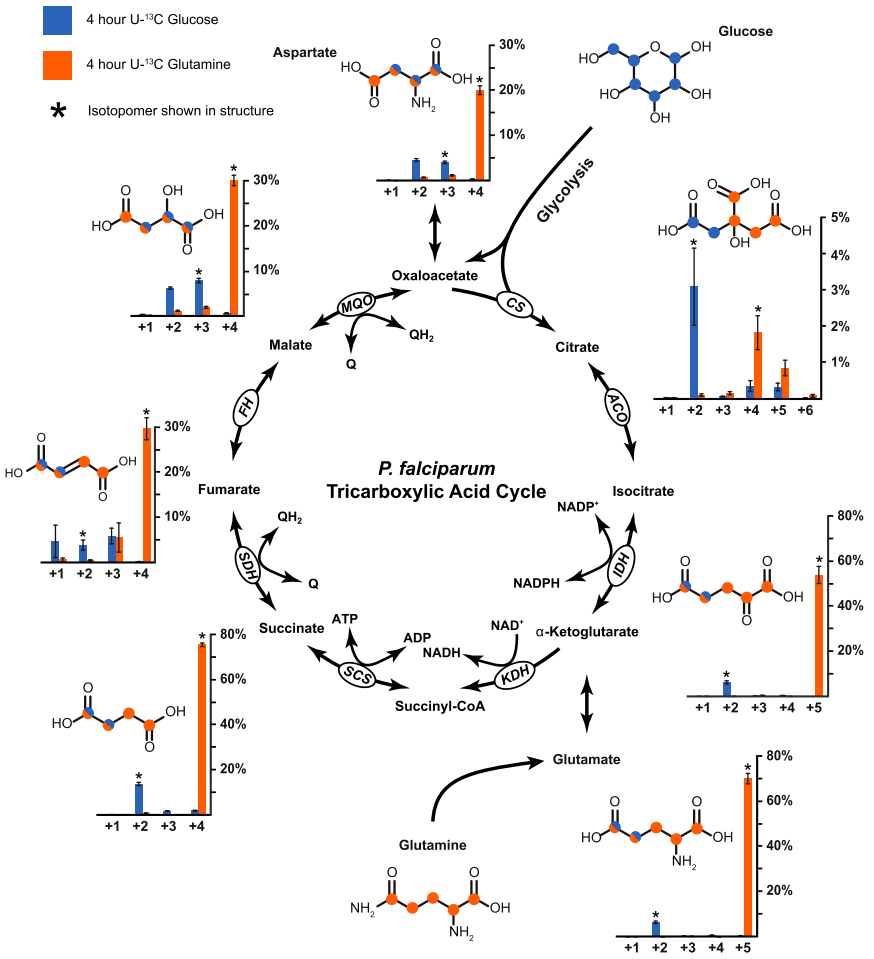

Figure 1. TCA Architecture in the Asexual Blood Stages of WT *P. falciparum*

Bar graphs show the percent isotopic enrichment (y axes) for ^{13}C isotopomers (x axes) of TCA metabolites extracted from D10 WT parasites incubated for 4 hr with either U-^{13}C glucose (blue bars) or U-^{13}C glutamine (orange bars). Please note different scales for distinct metabolites. These data are the average of three biological replicates, each carried out in triplicate. The molecular structures corresponding to the most-abundant glucose and glutamine-derived isotopomers are shown (*). Abbreviations: ACO, aconitase; CS, citrate synthase; FH, fumarate hydratase; IDH, isocitrate dehydrogenase; KDH, α-ketoglutarate dehydrogenase; MQO, malate quinone oxidoreductase; SCS, succinyl-CoA synthase; SDH, succinate dehydrogenase. Cofactors: NAD^+, nicotinamide adenine dinucleotide; NADH, reduced nicotinamide adenine dinucleotide; $NADP^+$, nicotinamide adenine dinucleotide phosphate; NADPH, reduced nicotinamide adenine dinucleotide phosphate; Q, ubiquinone; QH_2, ubiquinol. Error bars indicate SEMs of three biological replicates.

without associated metabolomic analyses. MacRae et al. (2013) conducted a metabolomic study of TCA and associated intermediates in *P. falciparum* combined with chemical inhibition of the single TCA enzyme aconitase. Disruption of *BCKDH* in *P. berghei* forced the parasite to grow in reticulocytes (Oppenheim et al., 2014); consequently, reticulocyte metabolites might influence metabolomic analysis of this KO line. Storm et al. (2014) investigated the role of phosphoenolpyruvate carboxylase (PEPC) in *P. falciparum* but did not directly follow the TCA cycle enzymes. Therefore, we undertook a study to look at the essentiality, redundancy, and functions of the TCA cycle enzymes in *P. falciparum*. Here, we generated 11 KO lines, disrupting six of the eight TCA cycle enzymes in *P. falciparum,* and analyzed phenotypic and metabolomic features of these KO lines in different life cycle stages. The availability of these KO lines also provides a resource for further detailed metabolic studies.

RESULTS

TCA Architecture in Wild-Type *P. falciparum*

To establish the baseline metabolic architecture of wild-type (WT) parasites, we incubated infected red blood cells (RBCs; D10 strain; ~90% parasitemia at the late trophozoite/schizont stages) in a culture medium containing either uniformly ^{13}C-labeled (U-^{13}C) glutamine or U-^{13}C glucose for 4 hr and monitored the appearance of ^{13}C in TCA intermediates by high-performance liquid chromatography-mass spectrometry (HPLC-MS). As controls, uninfected RBCs were labeled with U-^{13}C glutamine or U-^{13}C glucose for 4 hr. In agreement with a previous report (Ellinger et al., 2011), RBCs converted U-^{13}C glutamine into glutamate and α-ketoglutarate but no other TCA cycle intermediates (Table S2). Similarly, RBCs did not convert U-^{13}C glucose into TCA cycle intermediates during 4 hr incubations (Table S2). In contrast, WT parasites readily converted U-^{13}C glutamine into malate (Figure 1). The abundant +4 isotopomers (normal mass plus four atomic mass units) of succinate, fumarate, and malate observed indicated that TCA metabolism progressed through canonical oxidative reactions with the majority of carbon entering the cycle as α-ketoglutarate and leaving the cycle as malate (Figure 1). The presence of +4 citrate in these samples indicated that a small fraction of +4 malate was oxidatively converted into citrate. Oxidative turning of the TCA cycle was further confirmed by analyzing metabolites extracted from parasites incubated in U-^{13}C glucose. Mass spectrometry analysis showed low but significant isotopic enrichment in +2 citrate, +2 α-ketoglutarate, +2 succinate, +2 malate, and +2 aspartate (a proxy for oxaloacetate, as it is normally in equilibrium with aspartate via transamination; Shen, 2005; Figure 1). The presence of +2 isotopomers in these samples is consistent with glucose-derived acetyl-CoA entering the TCA cycle. The abundance of glucose-derived carbon in TCA cycle

intermediates was much lower than glutamine-derived carbon, indicating that glucose is a minor contributor to TCA flux in asexual blood stages (Figure 1). Similarly, the low intensity of the +5 citrate signal in U-^{13}C-glucose-labeled samples indicated that anaplerotic carbon input from glucose (i.e., oxaloacetate from cytosolic PEPC reaction) was small. Our results are in general agreement with the recent publications (Cobbold et al., 2013; MacRae et al., 2013; Storm et al., 2014) showing that blood-stage *P. falciparum* parasites carry out an oxidative TCA metabolism.

Most TCA Cycle Enzymes Are Dispensable in Asexual Blood Stages

To determine whether TCA cycle enzymes are essential for parasite survival, we attempted to knock out all eight TCA cycle enzymes through double crossover homologous recombination in D10 parasite line. We successfully knocked out six TCA enzymes, including genes encoding α-ketoglutarate dehydrogenase E1 subunit (Δ*KDH*; PF3D7_0820700), succinyl-CoA synthetase α subunit (Δ*SCS*; PF3D7_1108500), *SDH* flavoprotein subunit (Δ*SDH*; PF3D7_1034400), *CS* (Δ*CS*; PF3D7_1022500), aconitase (Δ*Aco*; PF3D7_1342100), and isocitrate dehydrogenase (Δ*IDH*; PF3D7_1345700; Figures S1 and S2). In addition, we also produced three double KO lines: (1) Δ*KDH*/Δ*SCS*, which should prevent glutamine-derived carbon from entering the canonical oxidative TCA cycle and block all of the biosynthetic routes to succinyl-CoA; (2) Δ*KDH*/Δ*IDH*, which should prevent utilization of glutamine-derived carbon in the TCA cycle; and (3) Δ*SCS*/Δ*SDH*, which should block oxidative turning of the cycle and substrate-level ATP generation in the mitochondrion (Figures S1 and S2). In contrast, we were unable to disrupt the genes encoding fumarate hydratase (*FH*; PF3D7_0927300) and malate quinone oxidoreductase (*MQO*; PF3D7_0616800), despite multiple trials using a variety of approaches (data not shown), suggesting that these two enzymes may be essential in the asexual blood stages.

To test the growth phenotypes of all nine KOs, we measured parasitemia over four or five generations (192–240 hr) relative to the WT (D10) parasites. Surprisingly, no significant growth defects were detected in any of the KO parasite lines when parasites were grown in complete RPMI-1640 medium (data not shown). To assess the possibility that growth defects may become apparent under nutritionally restrictive conditions, we also examined the growth phenotypes of the Δ*KDH*/Δ*IDH* and Δ*Aco* lines under various nutritional stresses (e.g., glucose, glutamine, and aspartate starvation) but found no differences between the KO and WT parasites (data not shown). These results show that TCA metabolism is not essential in asexual blood stages in vitro.

We also examined possible transcriptional alterations that may accompany the disruption of the TCA cycle during the intra-erythrocytic development cycle (IDC) in the Δ*KDH*/Δ*IDH* double-KO line. A whole genome expression profile was determined through microarray analysis of RNA extracted from tightly synchronized parasite cultures sampled every 6 hr over a 48 hr period. There were only 37 genes that had a statistically significant change at every time point over the 48 hr IDC (overall p across time < 0.002; Table S3). Although these variations were statistically significant, there were no clear coordinated changes in expression of TCA cycle or mitochondrial electron transport chain genes that could directly compensate for the genetic ablations of *KDH* and *IDH*.

Metabolic Consequences of TCA Cycle Disruptions in Asexual Blood-Stage Parasites

One possible explanation for the surprising absence of a growth phenotype in the KO parasite lines could be the presence of unannotated enzymes with redundant functions. To test this, we conducted a series of isotope-labeling experiments and used the diagnostic pattern of isotopomers to determine the metabolic capacity of the parasites using our nine KO lines. These experiments were conducted with U-^{13}C glutamine, because this amino acid is the main carbon source for the TCA cycle in WT parasites (Figure 1; Cobbold et al., 2013; MacRae et al., 2013). In general (but with some exceptions; see below), transgenic parasites incubated in U-^{13}C glutamine showed a consistent phenotype across the panel of TCA KO lines: metabolites upstream of the disrupted enzyme showed significant isotopic enrichment, whereas downstream metabolites showed significantly diminished levels of enrichment (Figure 2). The Δ*SDH* parasites, for example, accumulated +4 succinate ($p < 0.01$) but showed no appreciable production of +4 fumarate ($p < 0.001$) or +4 malate ($p < 0.001$). Similarly, the Δ*KDH* line, which interferes with the first committed step in TCA-related glutamine utilization, resulted in no detectable downstream labeling ($p < 0.001$ for all comparisons). These data show that *P. falciparum* does not contain redundant enzymes to bypass the deleted TCA enzymatic steps.

Although the majority of the parasite lines showed the anticipated metabolic accumulation upstream of the deleted enzymes, the Δ*SCS* and Δ*IDH* lines showed deviations from the overall pattern. In the case of the Δ*SCS* line, a reduced level of isotope labeling was observed in metabolites downstream of succinyl-CoA (Figure 2). Metabolic flux past the deleted enzyme could be attributable to the spontaneous conversion of succinyl-CoA to succinate (Simon and Shemin, 1953). In the Δ*IDH* line, parasites showed unexpectedly diminished levels of labeling in metabolites upstream of IDH (Figure 2), whereas the upstream flux in Δ*CS* and Δ*Aco* lines was not affected (Figure 2). The mechanisms behind the diminished levels of TCA intermediates in Δ*IDH* line are unclear at this point and need further investigation.

Mixing of Glucose- and Glutamine-Derived Carbon in the Mitochondrion

Citrate is a diagnostic metabolite of TCA metabolism that is only generated in the parasite mitochondrion. Our Δ*Aco* line is a convenient tool in this context because it accumulates citrate (Figure 2) and thus amplifies the mitochondrial signal. As shown in Figure S3, we incubated WT and Δ*Aco* parasites in medium containing 2-^{13}C glucose (only one carbon at position 2 is labeled) plus U-^{13}C glutamine and analyzed the isotopomer pattern of citrate. Infected cells incubated in the dual glucose/glutamine-labeled medium showed significant accumulation of +5 citrate ($p < 0.001$), which arises when glutamine-derived +4 oxaloacetate condenses with glucose-derived +1 acetyl-CoA (Figure S3). Importantly, these data also suggest that the two

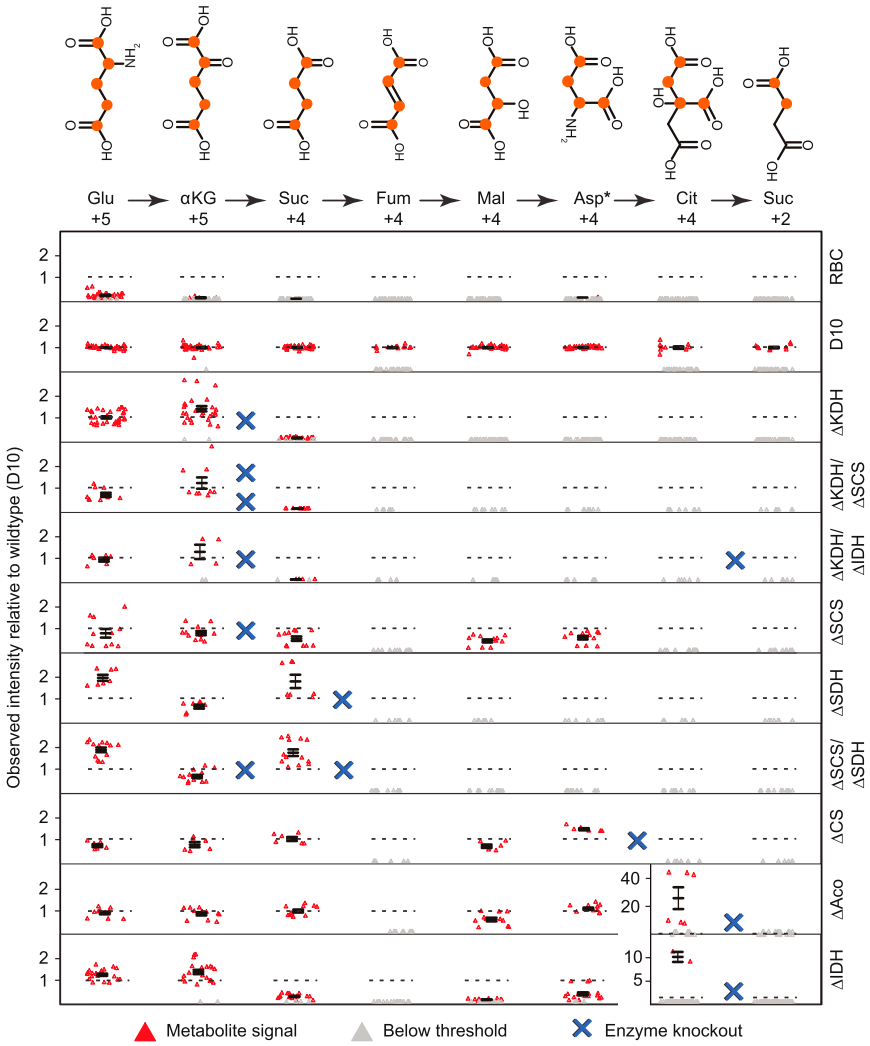

Figure 2. Metabolic Consequences of TCA Cycle Disruptions in the Asexual Blood Stages

(Top) A linearized depiction of oxidative TCA metabolism showing each of the expected isotopomers produced from U-^{13}C glutamine labeling. Among them, aspartate (Asp*) undergoes rapid exchange with oxaloacetate (oxaloacetate cannot be stably measured by the methods used in this work); +2 succinate (far right) is derived from a second round of the TCA cycle. Levels of isotopically enriched metabolites observed in extracts from uninfected RBCs, D10 WT, and nine different TCA KO lines are shown. For each line, data are averaged from at least three biological replicates, which were carried out in duplicate or triplicate. Each row shows a complete profile of the TCA cycle metabolites. Each column corresponds to the ratio of isotopomer in each KO line relative to the D10 WT. Orange circles show the positions of carbons labeled by U-^{13}C glutamine. Red triangles represent the ratio of each individual measurement relative to the D10 WT. Grey triangles indicate metabolites that are below the threshold of detection. Blue X's indicate the enzymatic steps that were disrupted in the KO lines. Abbreviations: αKG, α-ketoglutarate; Asp, aspartate; Cit, citrate; Fum, fumarate; Glu, glutamate; Suc, succinate; Mal, malate. Error bars indicate SEMs of at least three biological replicates. For genetic and phenotypic analyses of these KOs, see Figures S1 and S2 and Table S3.

carbon substrate, acetyl-CoA, is only derived from glucose (not from glutamine), most likely via the BCKDH reaction (Oppenheim et al., 2014).

Plasticity of TCA Metabolism in *P. falciparum*

Our glutamine labeling data showed that enzyme redundancy does not play a role in the survival of the TCA KO parasites (Figure 2). Another strategy that organisms can use to compensate for metabolic deficiencies is to increase the flow of carbon through alternative pathways. To test this possibility, we incubated parasites in U-^{13}C glucose and examined the isotope labeling of TCA-related metabolites. Glucose-derived carbon enters the TCA cycle via two classical mechanisms: (1) as two carbon acetyl-CoA units, which balance the two CO_2 molecules lost on each turn of the cycle, and (2) via anaplerotic reactions (i.e., PEPC reaction) that contribute four-carbon oxaloacetate or malate to the cycle (Cobbold et al., 2013; MacRae et al., 2013; Oppenheim et al., 2014; Storm et al., 2014).

Intracellular metabolites extracted from parasites grown in U-^{13}C glucose showed that TCA KO parasites (Δ*Aco*, Δ*KDH*, Δ*IDH*, Δ*KDH*/Δ*IDH*, and Δ*SDH*) accumulated the intracellular products of PEPC (i.e., +3 aspartate and +3 malate) to levels 1.7–5.3 times higher than those seen in the WT (Table S4; $p < 0.02$ for all pairwise comparisons to WT; $p = 0.06$ for Δ*Aco*). In addition, an analysis of metabolites excreted into the growth medium indicated that TCA KO parasites committed significantly more of their glucose-derived carbon to mitochondrial reactions ($p < 0.05$; Figure 3). As illustrated in Figure 3A, PEPC-derived metabolites can be divided into pre- and post-mitochondrial species, which can be differentiated on the basis of their isotopomer patterns. Pre-mitochondrial metabolites include +3 malate and +3 aspartate (as surrogate for +3 oxaloacetate), whereas post-mitochondrial metabolites include +5 citrate, +4/+5 α-ketoglutarate, and +4/+5 glutamate. The concentrations of these pre- and post-mitochondrial metabolites in the medium excreted by the D10 WT, Δ*KDH*, and Δ*KDH*/Δ*IDH* lines are shown in Figure 3B. In WT parasites, 89% of the excreted PEPC-derived carbon pool was pre-mitochondrial (+3 malate and +3 aspartate; Figure 3C). Thus, the majority of this potentially anaplerotic carbon pool was excreted without having been committed to mitochondrial reactions. In contrast, the KO lines committed significantly more of this glucose-derived carbon to mitochondrial reactions. As shown in Figure 3C, the percentages of post-mitochondrial metabolites in Δ*KDH* and Δ*KDH*/Δ*IDH* lines increased up to 3-fold in

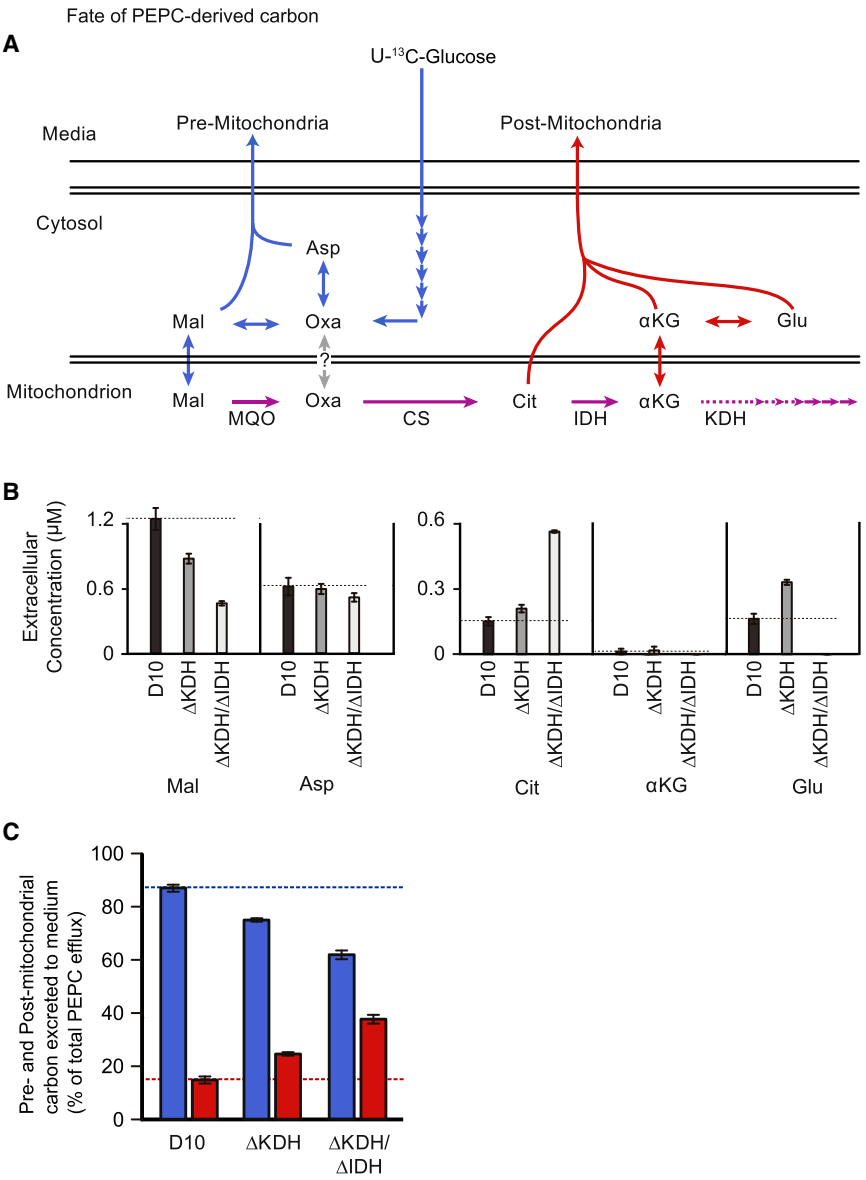

Figure 3. Anaplerotic Compensation for Impaired Glutamine Metabolism

(A) A schematic representation of the cytosolic and mitochondrial pathways used by PEPC-derived oxaloacetate. Blue arrows depict glucose utilization without mitochondrial participation (pre-mitochondrial flux), and red arrows indicate glucose utilization involving mitochondrial processes (post-mitochondrial flux).

(B) Extracellular concentrations of individual metabolites in D10 WT, Δ*KDH*, and Δ*KDH*/Δ*IDH* lines.

(C) Pre- and post-mitochondrial metabolites excreted into the medium by the D10 WT and various KO lines. The total excretion of glucose-derived carbon through PEPC is the sum of the concentrations of +3 malate and +3 aspartate (pre-mitochondrial, blue bars) and +5 citrate, +4/+5 α-ketoglutarate, and +4/+5 glutamate (post-mitochondrial, red bars). Data are derived from three biological replicates. Error bars indicate SDs of three biological replicates. The glucose labeling patterns in other TCA KO lines from the parasite pellet samples are shown in Figure S4 and Table S4.

comparison to the WT. In Δ*KDH* parasites, post-mitochondrial PEPC-derived carbon was excreted primarily as +4/+5 glutamate, whereas Δ*KDH*/Δ*IDH* primarily excreted +5 citrate (Figure 3B). This excretion pattern is consistent with the intracellular labeling patterns of these KO lines (Figure S4). These data showed that (1) parasites can draw on either glucose or glutamine as significant carbon sources for the TCA cycle, (2) parasites can secrete a variety of mitochondrial metabolites into the medium, and (3) KO parasites with impaired glutamine utilization commit a significantly higher proportion of their glucose-derived carbon to mitochondrial TCA reactions.

Mitochondrial Electron Transport Chain Inhibition Blocks Flux through the TCA Cycle

The mitochondrial electron transport chain is an established target of antimalarial drugs. To assess the connection between the TCA cycle and mitochondrial electron transport chain in *P. falciparum*, we conducted metabolic analyses in parasites under conditions where the mitochondrial electron transport chain was inhibited at complex III by atovaquone (Fry and Pudney, 1992; Srivastava et al., 1997). Atovaquone-treated parasites are unable to recycle ubiquinol to ubiquinone and thus become functional KOs for all ubiquinone-requiring enzymes including SDH, MQO, and dihydroorotate dehydrogenase (DHOD). Because atovaquone is toxic to WT parasites, these experiments were conducted with a mitochondrial-electron-transport-chain-independent transgenic line that expresses the cytosolic ubiquinone-independent *Saccharomyces cerevisiae* DHOD (yDHOD) (Ke et al., 2011; Painter et al., 2007). These parasites have a functional mitochondrial electron transport chain that can be inhibited by atovaquone but are able to grow in the presence of the drug because they generate pyrimidines via *yDHOD*. WT and y*DHOD*-transgenic parasite lines were treated with or without 100 nM atovaquone (~100 times EC_{50}) in medium containing U-^{13}C glucose for 4 hr. Labeling data showed that atovaquone-treated parasites did not assimilate glucose-derived carbon into TCA intermediates (Figure 4). The characteristic +2 isotopomers of TCA metabolites typically observed in control parasites were completely eliminated in atovaquone-treated parasites (Figures 4 and S5). Therefore, our data indicate that mitochondrial electron transport chain inhibitors prevent flux through the TCA cycle, as well as block the electron transport chain.

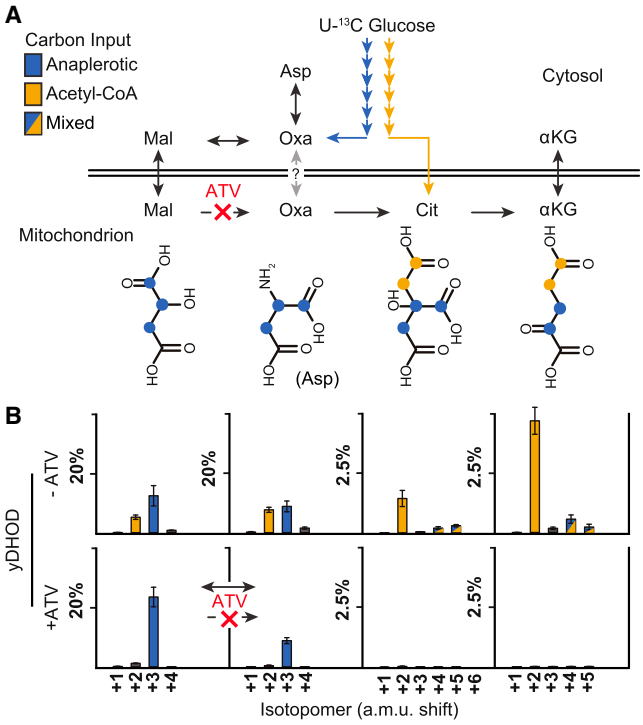

Figure 4. Mitochondrial Electron Transport Chain Inhibition Blocks the TCA Flux

(A) A schematic representation of carbon input from glucose into the TCA metabolites. Blue arrows/circles show anaplerotic input through PEPC reaction, whereas gold arrows/circles indicate flux from acetyl-CoA. Atovaquone (ATV) blocks the mitochondrial electron transport chain, thereby inhibiting MQO.

(B) Enrichment of each metabolite in *yDHOD* transgenic parasites in the presence or absence of ATV is shown. The +2 and +5 citrate isotopomers are diagnostic of flux through the citrate synthase reaction. Data are the average of three biological replicates. Error bars indicate SEMs of three biological replicates. A more comprehensive set of TCA cycle isotopomers is presented in Figure S5.

TCA Metabolism Is Essential for Malaria Transmission

All KO lines described above were derived from the *P. falciparum* D10 strain that is defective in sexual stage conversion. Therefore, we knocked out the *KDH-E1* and *Aco* genes, individually, in the gametocyte-producing NF54 strain. Disruption of *KDH* prevents glutamine-derived carbon from entering the TCA cycle, whereas *Aco* disruption blocks the full utilization of glucose as a TCA carbon source at an early step.

As observed for D10 lines, neither Δ*KDH* nor Δ*Aco* in the NF54 background exhibited growth defects in asexual stages (Figure S6A), suggesting that TCA metabolism is conserved among different parasite genetic backgrounds. When induced to generate gametocytes, NF54-Δ*KDH* and NF54-Δ*Aco* parasites behaved differently. NF54-Δ*KDH* was able to fully complete the gametocytogenesis process, forming mature stage V gametocytes in about 7–10 days (Figure S6B) with gametocytemia indistinguishable from that of WT NF54 (Figure 5A). In addition, there was no significant difference in the exflagellation profile of NF54-Δ*KDH* compared to the WT parasites (Figure 5B), suggesting that disruption of the TCA cycle did not harm gamete formation. Although the NF54-Δ*Aco* line progressed normally until stage III, it failed to form mature stage V gametocytes (Figures S6C and S6D). Overall gametocyte production in NF54-Δ*Aco* line was largely diminished as well (Figure 5D). Due to its lack of stage V gametocytes, NF54-Δ*Aco* did not form gametes (Figure 5E). Our observations confirm the role of *Aco* in gametocytogenesis and are consistent with the results observed when parasites were treated with 10 mM sodium fluoroacetate (NaFAc), which indirectly inhibits Aco (MacRae et al., 2013).

To assess the direct requirement of TCA flux and mitochondrial electron transport chain for exflagellation (gamete formation), mature WT NF54 parasites were incubated with atovaquone prior to exflagellation induction. As shown in Figure S6E, incubating mature WT gametocytes with 100 nM atovaquone for up to 24 hr had no effect on the parasite's exflagellation rate. These data indicate that mitochondrial electron transport chain and TCA fluxes are dispensable for male gamete formation by mature gametocytes. The absence of defects in NF54-Δ*KDH* parasites is also consistent with the conclusion that halting TCA metabolism is not harmful for gametocyte or gamete development. Thus, the defect in NF54-Δ*Aco* gametocytes may be due to reasons other than disruption of the TCA cycle (see Discussion).

To examine the role of TCA metabolism in mosquito stages, female *Anopheles gambiae* mosquitoes were fed with blood containing mature gametocytes derived from NF54 WT or NF54-Δ*KDH* parasites. The ability of parasites to mate successfully and develop further in the insect was assessed by counting oocysts in each mosquito 8 days after the blood feed. We found that none of the mosquitoes fed on blood with NF54-Δ*KDH* gametocytes produced oocysts, whereas those fed on blood containing WT gametocytes generated normal numbers of oocysts (Figure 5C). As expected, there were no oocysts formed in mosquitoes fed on NF54-Δ*Aco* gametocytes (Figure 5F), which fail to progress to mature gametocytes or gametes (Figure S6D). Because *KDH* disruption had no effect on gametocyte development and gamete formation (Figures 5A and 5B), the inability to form oocysts in this KO suggests that a fully functional TCA metabolism is only essential for parasite development in mosquitoes subsequent to gamete formation.

DISCUSSION

By combining genetic manipulation and metabolic analysis in unprecedented detail, this study significantly clarifies our understanding of TCA metabolism in the human malaria parasite, *P. falciparum*. The derivation of 11 KO lines also provides a resource for future investigations of the biological consequences of TCA cycle disruptions. Our study reveals several key findings, including (1) the TCA cycle is not essential for parasite survival in asexual blood stages but is required for parasite transmission; (2) the TCA metabolism can utilize different carbon sources and alter its pathway fluxes when the normal flux is disrupted; and (3) this metabolic plasticity is essential for parasites to meet bioenergetic demands in the multiple stages of their complex life cycle. A schematic representation of our principle findings is illustrated in Figure 6.

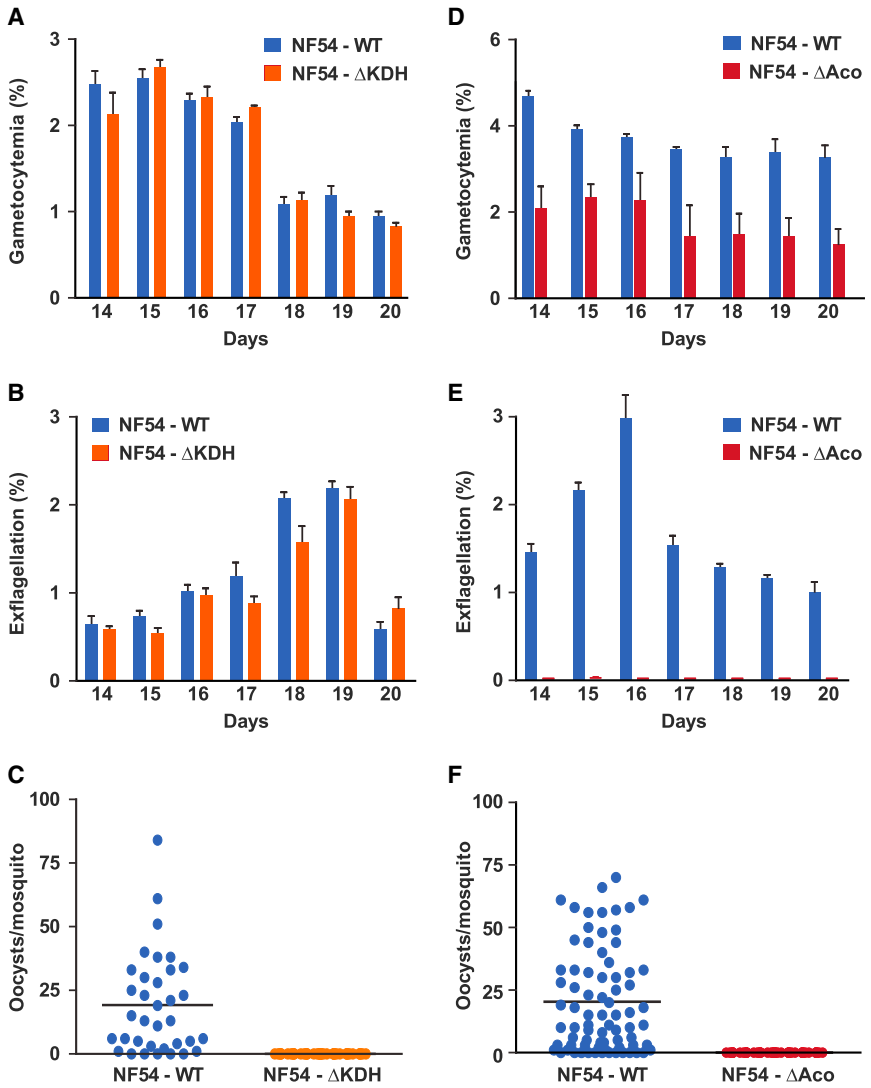

Figure 5. TCA Cycle Is Essential to Mosquito-Stage Development of *P. falciparum*

(A) Gametocytemia of NF54 WT and NF54-Δ*KDH* parasites on days 14–20 post-induction.

(B) Exflagellation percentage in NF54 WT and NF54-Δ*KDH* lines on days 14–20 post-induction.

(C) Infectivity of NF54 WT and NF54-Δ*KDH* parasites as measured by the number of oocysts per mosquito on day 8 after blood feeding.

(D–F) Results from NF54-Δ*Aco* line, corresponding to (A)–(C), respectively.

In (C) and (F), data are from two independent feeding experiments. Error bars indicate SEMs of three biological replicates. Morphological data are shown in Figure S6.

Our baseline metabolic data collected on WT parasites are in agreement with the current understanding of TCA cycle function in the parasite (Cobbold et al., 2013; MacRae et al., 2013; Oppenheim et al., 2014; Storm et al., 2014). Malaria parasites possess a canonical oxidative TCA cycle with the majority of TCA flux in asexual blood stages flowing from glutamine-derived α-ketoglutarate to malate (Figures 1, 2, and 6). Beyond these observations, we show that the parasite's mitochondrion can alter metabolic fluxes through alternative pathways when one route of carbon utilization is blocked. This metabolic plasticity was illustrated by our observations of substrate utilization in mutant lines lacking various TCA cycle enzymes (Figures 3, 6, and S4). Most TCA KO lines showed significant elevation in their utilization of glycolytically derived carbon in the remaining TCA reactions. In the extreme case of the *KDH* deletion, which prevents parasites from using glutamine as a carbon source for TCA reactions, parasites excrete glucose-derived glutamate into the medium (Figure 3). Thus, instead of the flow of carbon proceeding from glutamate to malate as in the WT (Figure 6A), in Δ*KDH* parasites, it proceeds from glucose-derived malate to glutamate, utilizing the *MQO* to *IDH* segment of the cycle (Figure 6C). This metabolic plasticity may allow multiple carbon sources to feed the TCA cycle at various times in the parasite's complicated life cycle.

A previous study in a related Apicomplexan parasite, *Toxoplasma gondii* (MacRae et al., 2012), provided evidence for a γ-aminobutyric acid (GABA) shunt, in which succinate is generated directly from α-ketoglutarate via the action of GABA α-ketoglutarate aminotransferase, glutamic acid decarboxylase, and succinic semialdehyde dehydrogenase enzymes. By extension, it has been proposed that a similar GABA shunt might also operate in *P. falciparum* (MacRae et al., 2013), although genes encoding all the requisite enzymes for the shunt cannot be detected in the *P. falciparum* genome. However, we found that the level of +4 succinate in the Δ*KDH* parasites labeled with U-^{13}C glutamine was very low (Figure 2), which would not be expected if a robust GABA shunt were to bypass the *KDH* reaction to feed the downstream TCA reactions. In light of the lack of evidence for GABA shunt enzymes in *P. falciparum,* we propose that the low level of +4 succinate in the Δ*KDH* line is likely a product of widely conserved α-ketoglutarate-dependent oxygenases, which generate succinate through iron- and oxygen-dependent decarboxylation of α-ketoglutarate (Schofield and Zhang, 1999). These enzymes carry out various protein hydroxylation and histone demethylation reactions, and genes encoding them are found in the *P. falciparum* genome (e.g., lysine-specific histone demethylase 1, PF3D7_1211600, and JmjC domain containing protein, PF3D7_0809900).

In asexual blood stages, parasites are remarkably resistant to disruption of TCA metabolism; six of the eight TCA cycle enzymes can be deleted with no detectable growth defects

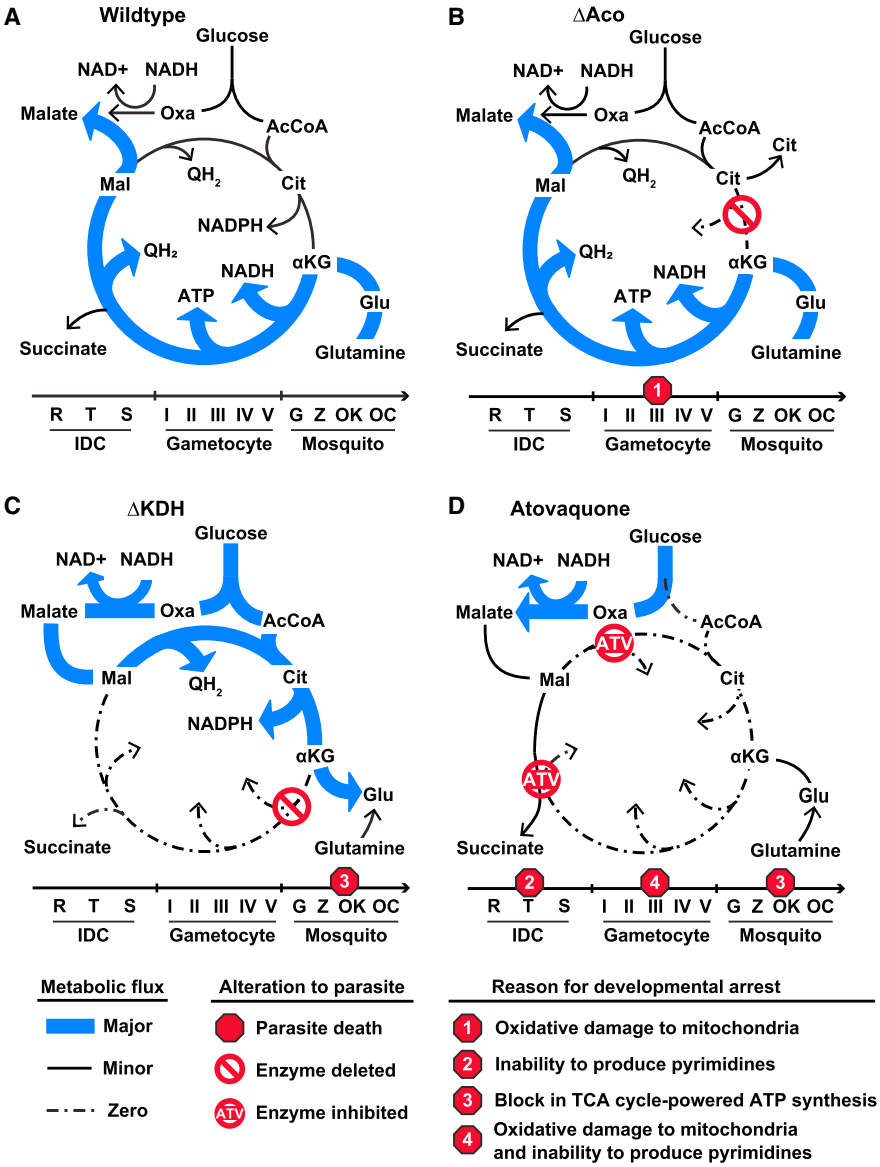

Figure 6. Models for TCA Metabolism under Various Conditions

A schematic representation of TCA flux is shown for (A) WT, (B) Δ*Aco*, (C) Δ*KDH*, and (D) atovaquone-treated parasites. Metabolic fluxes are depicted qualitatively as major (thick blue lines), minor (thin black lines), or zero (dotted lines). Some minor fluxes have been excluded for clarity of presentation. At the bottom of each panel, the progression of the parasite life cycle is indicated. IDC, intra-erythrocytic development cycle, is comprised of ring (R), trophozoite (T), and schizont (S). Gametocyte development progresses from stage I to stage V. Mosquito stages include gamete (G), zygote (Z), ookinete (OK), and oocyst (OC). Proposed reasons for developmental arrest at each of these stages are indicated by numbers within red octagons.

(data not shown). In the absence of redundancy (Figure 2), these data show that a full turning of the TCA cycle is not essential in asexual blood stages. The dispensability of TCA metabolism in blood stages extends to TCA-dependent pathways. For example, provision of succinyl-CoA via the TCA cycle to the heme biosynthetic pathway is not essential for blood-stage *P. falciparum* (Ke et al., 2014) or *P. berghei* (Nagaraj et al., 2013).

It was surprising to observe that disruption of the TCA cycle at the *KDH* step had no significant effect on sexual differentiation and gamete formation (Figure 5). Previous studies have shown upregulation of the TCA enzymes in gametocytes (Young et al., 2005), suggesting functional importance of the TCA cycle in gametocytogenesis. However, our results with the Δ*KDH* line indicate that a complete turning of the TCA cycle is not essential for sexual differentiation. In contrast, the parasite line lacking aconitase failed to produce mature gametocytes and gametes (Figure 5). Our results now provide genetic evidence to confirm the importance of aconitase in gametocytogenesis shown by MacRae et al. (2013). The specific necessity for aconitase for later gametocyte development might be due to the following

possible reasons: (1) aconitase is required for the production of mitochondrial NADPH, which is crucial for maintaining the mitochondrial redox balance and defense against oxidative damage and sustaining NADPH-dependent biosynthetic enzymes and (2) aconitase converts citrate to downstream metabolites, preventing the accumulation of citrate to a potentially toxic level. The fact that asexual stages of Δ*Aco* and Δ*IDH* parasites are not affected may suggest that the 48-hr life cycle is insufficient to produce lethal effects, whereas the 7–10 days required for gametocyte maturation results in accumulation of damage beyond the threshold of tolerability in the Δ*Aco* parasite.

In stark contrast to the asexual blood stages, parasite development in mosquitoes was completely inhibited by TCA cycle disruptions (Figure 5C). These results clearly establish the evolutionary necessity for maintenance of the TCA cycle by *P. falciparum*, because inhibition of transmission through mosquitoes would render the parasite extinct. This observation also suggests a major switch in mitochondrial functions as the parasite transitions from its vertebrate to invertebrate host. The motile ookinete has to survive outside a host cell for 24 hr and invade the mosquito midgut epithelium. Whereas blood-stage parasites are able to thrive through substrate-level generation of a mere two ATP molecules per glucose via glycolysis, survival in mosquitoes may place a much greater value on more economical energy generation through oxidative phosphorylation powered by the TCA cycle. In the Δ*KDH* line, input of TCA-derived electrons into mitochondrial electron transport chain would be significantly reduced, thereby decreasing mitochondrial oxidative efficiency, potentially causing parasites to arrest due to energy insufficiency. Observations of defective mosquito stage development by *P. berghei* with gene KOs of *SDH* (Hino et al., 2012), NADH dehydrogenase (Boysen and Matuschewski, 2011), and *BCKDH* (Oppenheim et al., 2014) also lend support to this argument.

Interestingly, we found that two of the TCA cycle enzymes, FH and MQO, could not be genetically ablated even in asexual blood stages. The inability to disrupt the *MQO* gene was surprising, because we have previously shown that biochemical activity of the enzyme could be functionally disrupted in *yDHOD* transgenic parasites (Ke et al., 2011; Painter et al., 2007). One possible reason could be an essential non-enzymatic structural function of MQO in mitochondrial biogenesis. This interpretation is supported by the observation that *MQO* is conserved among all apicomplexan parasites, including *Cryptosporidium* species, which have lost all other mitochondrial electron transport chain proteins (Abrahamsen et al., 2004). The essentiality of FH, on the other hand, could be explained by its role in a fumarate cycle serving the purine salvage pathway, as suggested by Bulusu et al. (2011). *Plasmodium* parasites are unable to synthesize purines and rely entirely on the purine salvage pathway. Two important enzymes in this pathway are adenylosuccinate synthetase and adenylosuccinate lyase. These enzymes utilize aspartate and generate fumarate in the process of converting inosine monophosphate to AMP. Mitochondrial FH could convert fumarate derived from purine salvage into malate in the mitochondrion, which could be transported to the cytosol and converted back to aspartate through successive reactions with malate dehydrogenase and aspartate aminotransferase. The fact that we can completely eliminate TCA-derived malate in several KO lines (Figure 2) suggests that the role of FH in the TCA cycle is dispensable. The essentiality of *FH* is, therefore, likely related to the requirements of the purine salvage pathway. It is interesting to note that two mitochondrial enzymes critical for parasite survival in blood stages, DHOD and FH, appear to serve pyrimidine biosynthesis and purine salvage, respectively.

Storm et al. (2014) found that *PEPC* could be knocked out but only when the parasites were provided with malate or fumarate in the medium. These authors suggested that PEPC is a key enzyme in *P. falciparum* central carbon metabolism by providing anaplerotic carbon for the TCA cycle. However, our Δ*Aco*, Δ*CS*, and Δ*IDH* lines grew normally despite their inability to incorporate anaplerotic carbon from glucose into downstream TCA reactions. Moreover, the survival of Δ*IDH* parasites indicates that mitochondrial NADPH production may not be essential in asexual blood stages, in contrast to the suggestion made by Storm et al. (2014). Consequently, we attribute the essentiality of *PEPC* to factors other than maintenance of the TCA cycle.

Our analysis of atovaquone-treated *yDHOD* transgenic parasites revealed another unexpected metabolic finding: oxaloacetate is evidently not transported into the mitochondrion, but malate is (Figures 4 and S5). This is surprising given that the parasite's mitochondrial dicarboxylate-tricarboxylate carrier (PfDTC) efficiently transports oxaloacetate in vitro (Nozawa et al., 2011). The absence of +2 and +5 citrate, despite normal levels of aspartate (observed as a surrogate for oxaloacetate), argues that PfDTC does not import oxaloacetate into the mitochondrion in vivo (Figures 4 and S5). Data from Δ*KDH*/Δ*IDH* line treated with atovaquone also support this argument (Figure S5); the residual signals (+2 and +5 citrate) were likely due to the delayed effect of atovaquone, which was added concurrently with ^{13}C-glucose to the culture during the 4-hr labeling. This observation also explains the parasite's propensity for secreting malate when using glutamine as a carbon source for TCA metabolism. Specifically, mitochondrial α-ketoglutarate/malate transport may be inherently linked through the action of an antiporter (presumably PfDTC).

It was interesting to note that, upon atovaquone treatment, the level of +3 succinate accumulated to a much-higher degree in D10 WT parasites when labeled with U-^{13}C glucose (Figure S5). Because input from glucose into the TCA cycle is inhibited under this condition, one potential source of +3 succinate could be a reverse reaction of *SDH* that reduces fumarate to succinate. Fumarate reductase activity was proposed by a previous study (Takashima et al., 2001). At this point, the nature of the electron donor for this reaction remains unclear, but it could be the high level of ubiquinol that would accumulate upon inhibition of the cytochrome bc_1 complex.

Our demonstration that the antimalarial drug atovaquone eliminated anaplerotic carbon input from glucose into TCA metabolism has implications for the potent efficacy of mitochondrial electron transport chain inhibitors in blocking transmission of parasites to mosquitoes (Fowler et al., 1994; Nilsen et al., 2013). Greater demand for mitochondrial contribution to bioenergetics in insect stages would make the mitochondrial electron transport chain, and the TCA cycle that primes it with reducing

equivalents, more critical for parasite survival. Our results show that mitochondrial electron transport chain inhibitors not only affect parasite respiration but also interfere with the TCA cycle (Figures 4 and S5). This assault on mitochondrial functions is the likely reason for the exquisite sensitivity of the mosquito stage development of parasites exposed in the mammalian host to mitochondrial electron transport chain inhibitors (Nilsen et al., 2013). Whereas our results clearly argue against potential TCA cycle inhibitors as antimalarial drug leads, because they are unlikely to inhibit blood-stage parasite growth, such compounds could serve as potent transmission-blocking agents. One TCA cycle enzyme with potential to be an attractive drug target is FH, inhibition of which would be effective at both vertebrate and invertebrate stages of the parasite. Selectively toxic compounds could be envisioned because the parasite possesses a type I FeS-dependent FH, which is substantially different from the human type II enzyme (Woods et al., 1988).

In summary, this study describes a comprehensive analysis of TCA cycle function in the human parasite *P. falciparum*. As shown in Figure 6A, malaria parasites maintain an oxidative TCA cycle with the main flux supplied by glutamine. In Δ*Aco* parasites (Figure 6B), maturation of gametocytes is prevented, perhaps due to an accumulation of damage related to the loss of mitochondrial NADPH production and/or high levels of citrate. In the Δ*KDH* line (Figure 6C), blood-stage parasites metabolize glucose into glutamate, whereas the insect-stage parasites fail to survive. Compounds targeting the mitochondrial electron transport chain, such as atovaquone, completely block the flux of metabolites through the TCA cycle (Figure 6D). Our study also reveals that the parasites have a flexible carbon metabolism, which may be important for making the transitions between the different environments encountered during the life cycle. In addition, the availability of 11 different KO lines described here provide an important resource for investigating biological consequences of disrupting the TCA cycle under various conditions, such as nutritional restrictions, in *P. falciparum*.

EXPERIMENTAL PROCEDURES

Gene KO Protocol

WT D10 and NF54 *P. falciparum* parasites were transfected with each KO construct and subjected to positive and negative selections. Deletion of the target gene was mediated via double crossover recombination.

Metabolite Labeling and HPLC-MS

Uninfected RBCs from heparinized blood were sedimented through 65% Percoll to remove any contaminated reticulocytes, platelets, and white blood cells prior to parasite culturing. Mycoplasma-free parasite cultures were tightly synchronized and grown to late trophozoite stage, and infected RBCs were isolated by density centrifugation using a Percoll step gradient (35%, 60%, and 65%). Purified parasites (late trophozoite to schizont stages) were incubated with the labeling medium for 4 hr. All of the isotopes used in this study (U-^{13}C glutamine, U-^{13}C glucose, and 2-^{13}C-glucose) were 99% pure and were purchased from Cambridge Isotope Laboratories.

Methanolic metabolite extracts were dried under a stream of N_2 gas and reconstituted in 200 μl (four times the original extraction volume) of HPLC-grade H_2O. High-resolution MS data were collected on a Thermo Scientific Exactive mass spectrometer in negative mode using ion-pairing C18 chromatography following previously published methods (Lu et al., 2010). Metabolite data were analyzed using MAVEN (Melamud et al., 2010), and isotopomers were corrected for naturally occurring ^{13}C using established methods (Fan et al., 2014). Data from technical replicates were averaged, and error bars report error across biological replicates. All p values were calculated by two-tailed t test. Raw data for all metabolites are provided in Table S5 (for U-^{13}C glutamine labeling of the wild-type and KO lines) and Table S6 (for multiple stable isotope labeling of the wild-type and selected KO lines).

For all other procedures, please see the Supplemental Experimental Procedures.

ACCESSION NUMBERS

All microarray data have been deposited to the NCBI GEO and are available under accession number GSE59015.

SUPPLEMENTAL INFORMATION

Supplemental Information includes Supplemental Experimental Procedures, six figures, and six tables and can be found with this article online at http://dx.doi.org/10.1016/j.celrep.2015.03.011.

AUTHOR CONTRIBUTIONS

This work was designed by A.B.V., H.K., M.W.M., M.L., and I.A.L.; H.K. and J.M.M. generated the KOs and conducted the isotope-labeling experiments and other analyses; and HPLC-MS and data analyses were performed by I.A.L. S.M.G. made *MQO* KO attempts. K.J.M. and M.J.-L. conducted mosquito-feeding experiments. H.J.P. analyzed the microarray data. H.K., I.A.L., M.W.M., M.L., and A.B.V. wrote the manuscript with input from all authors.

ACKNOWLEDGMENTS

We thank Dr. Praveen Balabaskaran Nina for providing the *SDH* KO construct and April M. Pershing for assistance with parasite culture. We thank Abhai Tripathi and Chris Kizito of the JHMRI Parasite and Insectary core facilities for their help. We also thank John Miller for help in creating Figures 1 and 6 and Jing Fan and Junyoung Park for their assistance with isotope correction. This project was funded by a grant from NIH (R01 AI028398) to A.B.V. and support from the Burroughs Welcome Fund, an NIH Director's New Innovators award (1DP2OD001315-01), and the Center for Quantitative Biology (P50 GM071508) to M.L.

Received: October 23, 2014
Revised: February 11, 2015
Accepted: March 4, 2015
Published: April 2, 2015

REFERENCES

Abrahamsen, M.S., Templeton, T.J., Enomoto, S., Abrahante, J.E., Zhu, G., Lancto, C.A., Deng, M., Liu, C., Widmer, G., Tzipori, S., et al. (2004). Complete genome sequence of the apicomplexan, Cryptosporidium parvum. Science *304*, 441–445.

Ariey, F., Witkowski, B., Amaratunga, C., Beghain, J., Langlois, A.C., Khim, N., Kim, S., Duru, V., Bouchier, C., Ma, L., et al. (2014). A molecular marker of artemisinin-resistant Plasmodium falciparum malaria. Nature *505*, 50–55.

Boysen, K.E., and Matuschewski, K. (2011). Arrested oocyst maturation in Plasmodium parasites lacking type II NADH:ubiquinone dehydrogenase. J. Biol. Chem. *286*, 32661–32671.

Bozdech, Z., Llinás, M., Pulliam, B.L., Wong, E.D., Zhu, J., and DeRisi, J.L. (2003). The transcriptome of the intraerythrocytic developmental cycle of Plasmodium falciparum. PLoS Biol. *1*, E5.

Bulusu, V., Jayaraman, V., and Balaram, H. (2011). Metabolic fate of fumarate, a side product of the purine salvage pathway in the intraerythrocytic stages of Plasmodium falciparum. J. Biol. Chem. *286*, 9236–9245.

Cobbold, S.A., Vaughan, A.M., Lewis, I.A., Painter, H.J., Camargo, N., Perlman, D.H., Fishbaugher, M., Healer, J., Cowman, A.F., Kappe, S.H., and Llinás, M. (2013). Kinetic flux profiling elucidates two independent acetyl-CoA biosynthetic pathways in Plasmodium falciparum. J. Biol. Chem. *288*, 36338–36350.

Ellinger, J.J., Lewis, I.A., and Markley, J.L. (2011). Role of aminotransferases in glutamate metabolism of human erythrocytes. J. Biomol. NMR *49*, 221–229.

Fan, J., Ye, J., Kamphorst, J.J., Shlomi, T., Thompson, C.B., and Rabinowitz, J.D. (2014). Quantitative flux analysis reveals folate-dependent NADPH production. Nature *510*, 298–302.

Fowler, R.E., Billingsley, P.F., Pudney, M., and Sinden, R.E. (1994). Inhibitory action of the anti-malarial compound atovaquone (566C80) against Plasmodium berghei ANKA in the mosquito, Anopheles stephensi. Parasitology *108*, 383–388.

Fry, M., and Pudney, M. (1992). Site of action of the antimalarial hydroxynaphthoquinone, 2-[trans-4-(4′-chlorophenyl) cyclohexyl]-3-hydroxy-1,4-naphthoquinone (566C80). Biochem. Pharmacol. *43*, 1545–1553.

Gardner, M.J., Hall, N., Fung, E., White, O., Berriman, M., Hyman, R.W., Carlton, J.M., Pain, A., Nelson, K.E., Bowman, S., et al. (2002). Genome sequence of the human malaria parasite Plasmodium falciparum. Nature *419*, 498–511.

Günther, S., McMillan, P.J., Wallace, L.J., and Müller, S. (2005). Plasmodium falciparum possesses organelle-specific alpha-keto acid dehydrogenase complexes and lipoylation pathways. Biochem. Soc. Trans. *33*, 977–980.

Hino, A., Hirai, M., Tanaka, T.Q., Watanabe, Y., Matsuoka, H., and Kita, K. (2012). Critical roles of the mitochondrial complex II in oocyst formation of rodent malaria parasite Plasmodium berghei. J. Biochem. *152*, 259–268.

Hodges, M., Yikilmaz, E., Patterson, G., Kasvosve, I., Rouault, T.A., Gordeuk, V.R., and Loyevsky, M. (2005). An iron regulatory-like protein expressed in Plasmodium falciparum displays aconitase activity. Mol. Biochem. Parasitol. *143*, 29–38.

Ke, H., Morrisey, J.M., Ganesan, S.M., Painter, H.J., Mather, M.W., and Vaidya, A.B. (2011). Variation among Plasmodium falciparum strains in their reliance on mitochondrial electron transport chain function. Eukaryot. Cell *10*, 1053–1061.

Ke, H., Sigala, P.A., Miura, K., Morrisey, J.M., Mather, M.W., Crowley, J.R., Henderson, J.P., Goldberg, D.E., Long, C.A., and Vaidya, A.B. (2014). The heme biosynthesis pathway is essential for Plasmodium falciparum development in mosquito stage but not in blood stages. J. Biol. Chem. *289*, 34827–34837.

Lu, W., Clasquin, M.F., Melamud, E., Amador-Noguez, D., Caudy, A.A., and Rabinowitz, J.D. (2010). Metabolomic analysis via reversed-phase ion-pairing liquid chromatography coupled to a stand alone orbitrap mass spectrometer. Anal. Chem. *82*, 3212–3221.

MacRae, J.I., Sheiner, L., Nahid, A., Tonkin, C., Striepen, B., and McConville, M.J. (2012). Mitochondrial metabolism of glucose and glutamine is required for intracellular growth of Toxoplasma gondii. Cell Host Microbe *12*, 682–692.

MacRae, J.I., Dixon, M.W., Dearnley, M.K., Chua, H.H., Chambers, J.M., Kenny, S., Bottova, I., Tilley, L., and McConville, M.J. (2013). Mitochondrial metabolism of sexual and asexual blood stages of the malaria parasite Plasmodium falciparum. BMC Biol. *11*, 67.

Melamud, E., Vastag, L., and Rabinowitz, J.D. (2010). Metabolomic analysis and visualization engine for LC-MS data. Anal. Chem. *82*, 9818–9826.

Nagaraj, V.A., Sundaram, B., Varadarajan, N.M., Subramani, P.A., Kalappa, D.M., Ghosh, S.K., and Padmanaban, G. (2013). Malaria parasite-synthesized heme is essential in the mosquito and liver stages and complements host heme in the blood stages of infection. PLoS Pathog. *9*, e1003522.

Nilsen, A., LaCrue, A.N., White, K.L., Forquer, I.P., Cross, R.M., Marfurt, J., Mather, M.W., Delves, M.J., Shackleford, D.M., Saenz, F.E., et al. (2013). Quinolone-3-diarylethers: a new class of antimalarial drug. Sci. Transl. Med. *5*, 77ra37.

Nozawa, A., Fujimoto, R., Matsuoka, H., Tsuboi, T., and Tozawa, Y. (2011). Cell-free synthesis, reconstitution, and characterization of a mitochondrial dicarboxylate-tricarboxylate carrier of Plasmodium falciparum. Biochem. Biophys. Res. Commun. *414*, 612–617.

Olszewski, K.L., Morrisey, J.M., Wilinski, D., Burns, J.M., Vaidya, A.B., Rabinowitz, J.D., and Llinás, M. (2009). Host-parasite interactions revealed by Plasmodium falciparum metabolomics. Cell Host Microbe *5*, 191–199.

Oppenheim, R.D., Creek, D.J., Macrae, J.I., Modrzynska, K.K., Pino, P., Limenitakis, J., Polonais, V., Seeber, F., Barrett, M.P., Billker, O., et al. (2014). BCKDH: the missing link in apicomplexan mitochondrial metabolism is required for full virulence of Toxoplasma gondii and Plasmodium berghei. PLoS Pathog. *10*, e1004263.

Painter, H.J., Morrisey, J.M., Mather, M.W., and Vaidya, A.B. (2007). Specific role of mitochondrial electron transport in blood-stage Plasmodium falciparum. Nature *446*, 88–91.

Phillips, M.A., Gujjar, R., Malmquist, N.A., White, J., El Mazouni, F., Baldwin, J., and Rathod, P.K. (2008). Triazolopyrimidine-based dihydroorotate dehydrogenase inhibitors with potent and selective activity against the malaria parasite Plasmodium falciparum. J. Med. Chem. *51*, 3649–3653.

Schofield, C.J., and Zhang, Z. (1999). Structural and mechanistic studies on 2-oxoglutarate-dependent oxygenases and related enzymes. Curr. Opin. Struct. Biol. *9*, 722–731.

Shen, J. (2005). In vivo carbon-13 magnetization transfer effect. Detection of aspartate aminotransferase reaction. Magn. Reson. Med. *54*, 1321–1326.

Simon, E.J., and Shemin, D. (1953). The preparation of S-succinyl coenzyme A. J. Am. Chem. Soc. *75*, 2520.

Srivastava, I.K., Rottenberg, H., and Vaidya, A.B. (1997). Atovaquone, a broad spectrum antiparasitic drug, collapses mitochondrial membrane potential in a malarial parasite. J. Biol. Chem. *272*, 3961–3966.

Storm, J., Sethia, S., Blackburn, G.J., Chokkathukalam, A., Watson, D.G., Breitling, R., Coombs, G.H., and Müller, S. (2014). Phosphoenolpyruvate carboxylase identified as a key enzyme in erythrocytic Plasmodium falciparum carbon metabolism. PLoS Pathog. *10*, e1003876.

Takashima, E., Takamiya, S., Takeo, S., Mi-ichi, F., Amino, H., and Kita, K. (2001). Isolation of mitochondria from Plasmodium falciparum showing dihydroorotate dependent respiration. Parasitol. Int. *50*, 273–278.

Takeo, S., Kokaze, A., Ng, C.S., Mizuchi, D., Watanabe, J.I., Tanabe, K., Kojima, S., and Kita, K. (2000). Succinate dehydrogenase in Plasmodium falciparum mitochondria: molecular characterization of the SDHA and SDHB genes for the catalytic subunits, the flavoprotein (Fp) and iron-sulfur (Ip) subunits. Mol. Biochem. Parasitol. *107*, 191–205.

Tanaka, T.Q., Hirai, M., Watanabe, Y., and Kita, K. (2012). Toward understanding the role of mitochondrial complex II in the intraerythrocytic stages of Plasmodium falciparum: gene targeting of the Fp subunit. Parasitol. Int. *61*, 726–728.

Tonkin, C.J., van Dooren, G.G., Spurck, T.P., Struck, N.S., Good, R.T., Handman, E., Cowman, A.F., and McFadden, G.I. (2004). Localization of organellar proteins in Plasmodium falciparum using a novel set of transfection vectors and a new immunofluorescence fixation method. Mol. Biochem. Parasitol. *137*, 13–21.

Vaidya, A.B., and Mather, M.W. (2009). Mitochondrial evolution and functions in malaria parasites. Annu. Rev. Microbiol. *63*, 249–267.

WHO (2013). World Malaria Report. http://www.who.int/malaria/publications/world_malaria_report_2013/report/en.

Woods, S.A., Schwartzbach, S.D., and Guest, J.R. (1988). Two biochemically distinct classes of fumarase in Escherichia coli. Biochim. Biophys. Acta *954*, 14–26.

Young, J.A., Fivelman, Q.L., Blair, P.L., de la Vega, P., Le Roch, K.G., Zhou, Y., Carucci, D.J., Baker, D.A., and Winzeler, E.A. (2005). The Plasmodium falciparum sexual development transcriptome: a microarray analysis using ontology-based pattern identification. Mol. Biochem. Parasitol. *143*, 67–79.

Cell Reports

Supplemental Information

Genetic Investigation of Tricarboxylic Acid Metabolism during the *Plasmodium falciparum* Life Cycle

Hangjun Ke, Ian A. Lewis, Joanne M. Morrisey, Kyle J. McLean, Suresh M. Ganesan, Heather J. Painter, Michael W. Mather, Marcelo Jacobs-Lorena, Manuel Llinás, and Akhil B. Vaidya

Supplemental Experimental Procedures

1. Plasmid construction.

The plasmids pCC1, pCC4 and pUF-1, possessing the selectable marker genes human dihydrofolate reductase (*hdhfr*), blasticidin deaminase (*bsd*) and yeast dihydroorotate dehydrogenase (*yDHOD*), respectively, confer resistance to 5 nM WR99210, 2.5 µg/ml blasticidin, and 1.5 µM DSM1, respectively. They share the same negative selection marker, the *FCU* gene (yeast cytosine deaminase/uracil phosphoribosyl transferase), which confers sensitivity to 5-fluorocytosine (5-FC, 2 µM). We cloned 500-1000 bp 5' and 3' flanking homologous sequences (5'f, 3'f) from each gene into a PCR cloning vector (Stratagene) and the sequences were confirmed (Genewiz). After restriction digestion with restriction endonucleases (New England Biolabs), the 5'f and 3'f sequence fragments were purified from agarose gels and cloned into pCC1, pCC4 or pUF-1. The 5'f and 3'f fragments from *KDH-E1* (α-ketoglutarate dehydrogenase E1 subunit, PF3D7_0820700), *SCS-α* (succinyl-CoA synthetase α subunit, PF3D7_1108500), *FH* (fumarate dehydrogenase, PF3D7_0927300), *MQO* (malate quinone oxidoreductase, PF3D7_0616800), *CS* (citrate synthase, PF3D7_1022500), *Aco* (aconitase, PF3D7_1342100), and *IDH* (isocitrate dehydrogenase, PF3D7_1345700) were each cloned into pCC1. *KDH-E1* fragments were also cloned into pCC4. *SDH-Fp* (succinate dehydrogenase flavoprotein, PF3D7_1034400) fragments were cloned into pUF-1. Primers for PCR amplifications are shown in Table S1.

2. Parasite lines, parasite culture and transfection methods.

P. falciparum D10 was the primary parental wildtype line used for gene knockout experiments. *P. falciparum* NF54 was used for gametocyte studies and mosquito feedings. Parasites were cultured in human O^+ erythrocytes (5% hematocrit) in RPMI 1640 medium containing 0.5% AlbuMax and incubated at 37 °C in an incubator filled with a blood gas mixture (89% N_2, 5% CO_2, 6% O_2). Transfections were carried out by standard methods. Briefly, ring-stage parasites were washed three times with warm incomplete cytomix and resuspended in an equal volume of ice cold incomplete cytomix at 50% hematocrit. A 250 µl parasitized erythrocyte suspension was mixed with 50 µg plasmid in a 0.2 cm cuvette, and electroporated using a BioRad

Genepulser set at 0.31 kV, 960 μF. Cultures were maintained under the appropriate selective pressure (5 nM WR99210, 2.5 μg/ml blasticidin, and/or 1.5 μM DSM1), starting 48 h post electroporation.

3. Parasite cloning.

Cloning was done by limiting dilution. One ml of culture was diluted with 9 ml medium to make a 1:10 parasitized erythrocyte stock. The erythrocyte cell density of the stock (cells/ml) was determined by a hemocytometer. The number of parasitized erythrocytes per ml (pRBC/ml) in the stock was determined by multiplying the cell density by the parasitemia. The stock was diluted by serial dilutions in medium containing uninfected erythrocytes at 3% hematocrit to final concentrations of 2.5 and 0.5 pRBC/ml. The final dilutions were plated into 96 well plates at 0.2 ml per well to provide an average of 0.5 and 0.1 pRBC/well. The diluted cultures in these plates were split 1:2 every 9 days during the first 3-4 weeks. At the 3rd split, one half of the culture in each well was transferred to a new plate and continued in culture, while the other half was maintained in the original plate and pulsed with 150 μl of low-hypoxanthine medium containing 1 μCi ^{3}H-hypoxanthine for 24 h. ^{3}H-hypoxanthine incorporation into nucleic acids was determined by a TopCount^{TM} radiation counter (PerkinElmer). The wells with relatively high radioactivity were checked by thin blood smears, and those with confirmed parasite growth (positive clones) were expanded in culture for further characterization.

4. DNA isolation, RNA isolation, PCR and RT-PCR.

DNA was isolated from mixed-stage parasites using the QIAamp DNA Blood Mini kit (Qiagen). RNA was isolated from mixed-stage parasites using the RNAgents RNA isolation kit (Promega). Purified RNA was treated with RNase free DNaseI (New England Biolabs) in the presence of RNase inhibitor (Promega) for 30 min at 37 ^{o}C to eliminate any contaminating DNA. The treated RNA was then recovered using an RNeasy Mini Kit (Qiagen). cDNA was synthesized from 2 μg RNA by Avian Myeloblastosis Virus Reverse Transcriptase (Promega) using Oligo(dT)$_{15}$ as the primer, followed by PCR with gene-specific primers. Two μl of reverse transcriptase product served as template for each cDNA PCR reaction.

PCR reaction was set up in a 25 µl volume with the following conditions: 2.5 µl 10x buffer, 2 µl forward primer (10 µM), 2 µl reverse primer (10 µM), 0.5 µl 10 mM dNTP, 0.5 µl Polymerase, 2 µl of DNA (50-100ng) and 15.5 µl sterilized deionized water. For diagnostic PCRs, the thermal cycling program was generally set as follows: 2 min at 94^{o}C, 30 cycles of 94^{o}C for 30 sec, 50^{o}C for 45 sec and 60^{o}C for 4 min, and a final extension at 65 ^{o}C for 10 min. For plasmid constructions, Vent or Pfu Polymerase (New England Biolabs or Stratagene) was utilized, and the extension time for each cycling was set according to the length of the DNA to be amplified. For RT-PCRs, the extension time for each cycling was set at 1 min. Primers of PCRs and RT-PCRs are shown in Table S1.

5. Southern blot analysis.

For each parasite sample to be analyzed, 3 µg genomic DNA were digested by the appropriate restriction endonucleases (New England Biolabs) overnight. Southern blot transfer and hybridization was then carried out using a standard protocol [1]. The DNAs were separated on a 0.8% agarose gel and transferred to Gene Screen Plus^{TM} membrane (PerkinElmer) by the high salt capillary transfer method. Probes were PCR amplified, cleaned and labeled with [α-^{32}P]dATP (PerkinElmer) using a Prime-It II Random Primer Labeling Kit (Stratagene). The blot was hybridized with the labeled probes, washed and exposed to film at -80 ^{o}C in a cassette overnight, before being developed.

6. Northern blot analysis.

Northern blots were performed using standard methods. Aliquots of 20 µg total RNA were separated by denaturing formaldehyde agarose gel electrophoresis. To confirm equal loading of RNA from different samples, an additional 5 µg of each RNA sample was loaded in the same gel parallel to the lanes containing 20 µg RNA. These loading control lanes (5 µg/lane) were cut off, stained with ethidium bromide, visualized under UV light and photographed with an Eagle Eye imaging system (Stratagene). Transfer of RNA to Gene Screen Plus^{TM} membrane, probe labeling, hybridization and autoradiography proceeded as described above for the Southern blot procedure.

7. Growth curves.

Wildtype and knockout parasites were tightly synchronized using 0.5 M Alanine/10 mM Hepes (pH 7.5) [2] and adjusted to 1% parasitemia on day 0 at ring stage. Parasitemia was monitored daily from 1000 RBCs on thin

blood smears over 8 to 10 days (4-5 intraerythrocytic life cycles). On days 2, 4, 6, and 8, cultures were split 1:5. Growth Index (Y-axis) was calculated as the product of the parasitemia and the splitting factors.

8. Metabolite labeling.

a) Preparation of uninfected RBCs used in labeling experiments. Heparinized blood was used for culturing parasites in the labeling experiments to avoid citrate contamination, which is present in CPD (Citrate Phosphate Dextrose) blood. Following three washes with PBS, the uninfected erythrocytes were resuspended in PBS to make 30% hematocrit and centrifuged through a 65% Percoll cushion (GE Healthcare Biosciences) (15 ml 65% Percoll topped with 35 ml of 30% hematocrit blood) to remove any contaminated reticulocytes, platelets, and white blood cells. The erythrocyte pellets were collected, washed with PBS thoroughly, and resuspended in complete RPMI-1640 medium for future use.

b) Parasite culture and synchronization. Parasites (wildtype and knockout lines) were tightly synchronized at least three times by treatment with 0.5 M Alanine/10 mM Hepes (pH 7.5). 48 h after the first synchronization, the second and the third synchronizations were done with a 12 h interval. The cultures were expanded in 3-4 T75 flasks for each line.

c) Percoll gradient purification. When the parasites were late stages, the infected erythrocytes were harvested, resuspended to 20-30% hematocrit in complete RPMI 1640 medium and centrifuged through a Percoll step gradient (from bottom to top: 10 ml of 65%, 13 ml of 60%, 8 ml of 35% Percoll and 18 ml of infected erythrocyte suspension). The parasite-containing layer at the interphase of the 65% and 60% Percoll was collected, washed twice with PBS, and resuspended in the labeling medium. The labeling medium was composed of RPMI-1640 complete medium in which one or two components (glutamine, glucose) had been replaced by ^{13}C heavy isotope labeled isomer(s) (Cambridge Isotope Laboratories, Inc.). For each line, 100-150 µl purified infected erythrocyte pellet was resuspended in 10-15 ml labeling medium, incubated at 37 ^{o}C for 4 h and divided into two or three replicates upon harvesting.

d) Metabolite extraction. Following labeling, cells were spun down by centrifugation (1000 rpm, 5 min, RT). The supernatant was collected, centrifuged again at top speed for 1 min to remove debris, and mixed with 4

volumes of methanol (-80 ^{o}C) and stored at -80 ^{o}C. For each ~50 µl parasite pellet, 200 µl methanol (-80 ^{o}C) was directly added and immediately vortexed vigorously. Samples were incubated on dry ice for 15 min with vortexing every 5 min. The pellet was spun down at a low speed (500 rcf, 5 min, 4 ^{o}C). The supernatant was removed to a clean Eppendorf tube and stored on dry ice. The pellet was resuspended in 500 µl 80% methanol (4 ^{o}C) and sonicated in an ice water bath for 15 min in an FS30H bath sonicator (Fisher Scientific). After sonication, the pellet was spun down (15,000 rcf, 5 min, 4 ^{o}C) and the supernatant was removed and combined with the previous aliquot. The pooled supernatants were centrifuged again at 15,000 rcf, 5 min, 4 ^{o}C to remove any residual cell debris.

9. Whole-genome microarray analysis over the 48 h IDC. Both Δ*KDH*/Δ*IDH* and D10 parasites were tightly synchronized and maintained at a high parasitemia (~15%). Samples were collected over the time course at 0, 6, 12, 18, 24, 30, 36, and 42 h. Zero h indicates the synchronization start point (parasites are early rings). Cells were harvested from 100 ml of culture suspension at each time point (200 ml for time points 0 and 6) by centrifugation. Total RNA was extracted and purified using TriZol reagent (Invitrogen) in 4 volumes of reagent to 1 volume of packed parasitized erythrocytes as previously described [3]. cDNA was generated from total RNA of each time point sample, dye coupled and hybridized to *P. falciparum* 8x15K Agilent Arrays as previously described [4, 5]. Hybridized arrays were then scanned using an Agilent G2505B Microarray Scanner (Agilent Technologies) with 5 µm resolution at wavelengths of 532 nm (Cy3) and 633 nm (Cy5) employing an extended dynamic range (10-100%) setting. Normalized intensities were extracted using Agilent Feature Extractor Software Version 9.5 by the standard protocol and uploaded to the Princeton University Microarray Database (PUMA.princeton.edu) for analysis.

10. Gametocyte induction and exflagellation. Asynchronous asexual stage NF54 cultures (wildtype and knockout lines) at 5-10% parasitemia were split to initiate gametocyte cultures at 0.5% parasitemia and 2.5% hematocrit in a 50 ml culture on day 0. The standard RPMI-1640 medium was supplemented with 10% human serum (O^{+}). The cultures were fed every day without being split and Giemsa-stained thin blood smears were prepared and counted daily. On days 14 to 20 post induction, for each parasite culture, the total number of erythrocytes was determined by a hemocytometer. The total number of gametocytes in each culture was then calculated by multiplying gametocytemia with the total number of erythrocytes. On each of these days, 1 ml

culture was removed, centrifuged quickly (3,000 rpm, 2 min) and resuspended in 200 µl of exflagellation medium containing 25% human serum (O^+), 50 µM xanthurenic acid [6] at pH 8.4. After 10 min of incubation at room temperature, a 10 µl cell suspension was pipetted onto a hemocytometer and the number of exflagellating centers was counted using a standard optical microscope (20x objective) during the next 20 min. The total number of exflagellating centers in each culture was then calculated, and the percentage of exflagellation was determined by dividing the total number of exflagellating centers by the total number of gametocytes in each culture.

11. Plasmodium infection in mosquitoes. Mosquito maintenance and *P. falciparum* infection were carried out according to Smith et al. [7]. Briefly, day 18 gametocyte cultures were diluted to 0.2% stage V gametocytemia in 50% hematocrit blood/human serum. Approximately 60 female *A. gambiae* mosquitoes (Keele strain, obtained from Drs. Hilary Hurd and Paul Eggleston at Keele University) were fed on each gametocyte culture for 1h using glass membrane feeders connected to a 37 °C circulating water bath. Non-fed mosquitoes were separated from fed mosquitoes 24 h after feeding. Eight days post-feeding, mosquito midguts were dissected and stained with 0.1% mercurochrome for 30 min. Oocysts per midgut were counted by visualizing midguts under the 10x objective of a compound microscope.

Supplemental References

1. Sambrook, J. and D. Russell, *Molecular cloning: a laboratory manual.*, in *3rd edition*. 2001, Cold Spring Harbor Laboratory Press.
2. Haynes, J.D. and J.K. Moch, *Automated synchronization of Plasmodium falciparum parasites by culture in a temperature-cycling incubator.* Methods Mol Med, 2002. **72**: p. 489-97.
3. Bozdech, Z., et al., *The transcriptome of the intraerythrocytic developmental cycle of Plasmodium falciparum.* PLoS Biol, 2003. **1**(1): p. E5.
4. Painter, H.J., et al., *Whole-Genome Analysis of Plasmodium spp. Utilizing a New Agilent Technologies DNA Microarray Platform.* Methods in molecular biology, 2013. **923**: p. 213-9.
5. Kafsack, B.F., H.J. Painter, and M. Llinas, *New Agilent platform DNA microarrays for transcriptome analysis of Plasmodium falciparum and Plasmodium berghei for the malaria research community.* Malaria Journal, 2012. **11**: p. 187.
6. Billker, O., et al., *Identification of xanthurenic acid as the putative inducer of malaria development in the mosquito.* Nature, 1998. **392**(6673): p. 289-92.
7. Smith, R.C., et al., *Regulation of anti-Plasmodium immunity by a LITAF-like transcription factor in the malaria vector Anopheles gambiae.* PLoS Pathog, 2012. **8**(10): p. e1002965.

Supplementary Tables:

Table S1. **Primers used in this study, related to Experimental Procedures.**

Gene	Primer ID	Primer Sequence[a]	Purpose
KDH-E1	5fPfKDHNcoIF	ATccatggCCTTTTAGAAACAATTTACACAAATCG	**knockout construct cloning**
	5fPfKDHEcorIR	GTgaattcCATAATAATCAATTTCAACACCTAAATGG	
	3fPfKDHSpeIF	GAactagtCATTAAAAACACCACATACCATAG	
	3fPFKDHSacIIR	ATccgcggAGGTATATTTTTGAACATGCATG	
SCS-α	PfSCSNc01	CAccatggCTATTTTTGCTTATCTTTGATATATCAG	
	PfSCSER02	GTgaattcTGACGTGAAATTATTTAAATAAATAGCATACTG	
	PfSCSSP03	GAactagtCCCAATTGTCCTGGAATC	
	PfSCSSc04	AAccgcggTCATAATAAAGAATATGTATTAAAAAATTGTTGG	
SDH-Fp	sdhA01	CAcctaggCAAATGTTCCCGTGTGG	
	sdhA02	ATccatggCCTGTTCTATCAGCAGCG	
	sdhA03	GAactagtGAGCAAATCGGTTAGGAGC	
	sdhA04	AAccgcggTCATATGAGCATATTAAGAAATGTCTTC	
FH	5fPfFHNcoIF	CTccatggTCTCATCTCATTTGAAGCATTTTTACAAG	
	5fPfFHEcorIR	CTgaattcACATAGCCACATATTTATCATTTTTACTTG	
	3fPfFHSpeIF	GAactagtGAAAAAATTATTCTACAGAAAGCTC	
	3fPfFHSacIIR	ATccgcggTAACCATTTATTATAAAAATCATTGCCTTTG	
MQO	PfMQO5fF	ATccatggTCTTCACACTGTGTTAGAGGAATACA	
	PfMQO5fR	CTgaattcTGGCTTTTTCAAAAGAATAATTGG	
	PfMQO3fF	GTactagtGGACCAACAGCTATACCTTTACCA	
	PfMQO3fR	ATccgcggAAATGAATAAGTGGAACATATGGAA	
CS	5fFCSFNcoI	CTccatggCAATCCATCACATATAATATG	
	5fRCSREcoRI	ATgaattcCCATAGGATATTCACAAGTAT	
	3fFCSFSpeI	CTactagtATCCATATTTGTCCTATTCTG	
	3fRCSRSacII	ATccgcggGTTCATCATATATATTTTATTC	
ACO	5fFACONcoI	CTccatggCACACATAAGTTGATACATAC	
	5fRACOEcoRI	ATgaattcATACCCCATTTAAG	
	3fFACOSpeI	CTactagtTAGCTTCTCCGGTATTAGTTG	
	3fRACOSacII	ATccgcggCCTTTCTTCAATTTCGGTATC	
IDH	5fPfIDHNcoIF	GAccatggATCATCTTTATTTTTAGCGCACAC	
	5fPFIDHEcorIR	CTgaattcCTTTAACTCTTGCAGCATCAGG	
	3fPfIDHSpeIF 3fPfIDHSacIIR	GAactagtGCATGGACCAAAGGATTAGAAC TAccgcggCAACTATGTTAAGGATAATACAGTATTG	
KDH-E1	5foutKDH	AGAAGACAGGTATAATGTGCAAC	**Diagnostic PCR**
	3foutKDH	GTATTTACGTGTGTTTATTTGGATATACC	
SCS-α	PfSCSa5prtst01	GGAGCATCCTTACTTTAGAGAAG	
	PfSCSa3prtst02	CATTAAGTTAACAATTATAAAAAGCACTGAAG	
SDH-	5foutSDH	TTGCATTGTATTTGAAAAAGAGAGAG	

Fp	3foutSDH	CTGACCAAACAAATAAAGAATAGTTTAC	
FH	5foutFH	CGGCATATTAATGTTATACCAATCC	
	3foutFH	GCACTTGCGAAATTTGGGTT	
MQO	5foutMQO	GTTTGTATATCTTAATTTTTGAAGGTACACAC	
	3foutMQO	CTGATATTATATACAAATAGGAGATTTTCAAAGAC	
CS	5foutCS	GATTTTAATTTTTCCCATAAGACTTG	
	3foutCS	GAAAATTTTACTGAACTCTTTGG	
ACO	5foutACS	GTTTGTGTAGTGTATTTCTTTTTTG	
	3foutACS	CGTTCTTCTTATCGATTACATAT	
IDH	5foutIDH	CTCCTGCTCATCAAAATGATAAATATG	
	3foutIDH	TGGGAAAATTGTATTGCCTCA	
KDH-E1	RT-KDHE1-F	TTTTCTCATCGACACGCAGT	**RT-PCR**
	RT-KDHE1-R	CATTTGTCTTCTTAATGCATGG	
SCS-α	RT-SCS-F	CCAAGGAAGAAAGGCACAAC	
	RT-SCS-R	AACTTTAGTTGTTTGATTAACTCC	
SDH-Fp	RT-SDH-F	AATGAATGTATTGGGGTAATCTGT	
	RT-SDH-R	TACATCAACTCCCGCAAAAA	
CS	RT-CS-F	CCAGCTGTAGATGACTTAAAAC	
	RT-CS-R	TCAAATGTGATACATGTGCAC	
ACO	RT-ACO-F	TTTGAAGGCAGAGTCCATCC	
	RT-ACO-R	GTATCATTCCAGCCGGTGAT	
IDH	RT-IDH-F	AGACATGCATATGCTGATCAAT	
	RT-IDH-R	CCTTGAGCAACAGCATCAGA	

[a]restriction endonuclease sites are shown in lower case letters.

Table S2. The profile of TCA metabolites in red blood cells labeled with U-^{13}C-glucose or U-^{13}C-glutamine for 4 h, related to Figure 1.

	C12 (%)	+1 (%)	+2 (%)	+3 (%)	+4 (%)	+5 (%)	+6 (%)
Glu	99.99±0.01	0.00±0.00	0.00±0.00	0.00±0.00	0.00±0.00	0.00±0.00	
	95.22±0.10	0.10±0.10	0.04±0.02	0.04±0.01	0.02±0.00	4.57±0.02	
aKG	99.97±0.05	0.00±0.00	0.00±0.00	0.00±0.00	0.01±0.02	0.01±0.02	
	71.57±5.84	0.00±0.00	0.69±1.38	0.00±0.00	0.00±0.00	27.74±5.78	
Suc	99.80±0.24	0.17±0.20	0.01±0.01	0.01±0.01	0.01±0.01		
	99.76±0.25	0.00±0.00	0.00±0.00	0.00±0.00	0.24±0.25		
Fum	100.00±0.00	0.00±0.00	0.00±0.00	0.00±0.00	0.00±0.00		
	99.98±0.02	0.00±0.00	0.00±0.00	0.01±0.01	0.01±0.01		
Mal	99.99±0.00	0.00±0.00	0.00±0.00	0.00±0.00	0.00±0.00		
	99.99±0.01	0.00±0.00	0.00±0.00	0.01±0.00	0.00±0.00		
Asp	99.97±0.02	0.00±0.00	0.01±0.00	0.01±0.01	0.01±0.01		
	99.20±0.16	0.73±0.16	0.01±0.00	0.03±0.00	0.03±0.00		
Cit	99.96±0.04	0.00±0.00	0.01±0.01	0.01±0.01	0.01±0.01	0.01±0.01	0.01±0.01
	99.97±0.00	0.00±0.00	0.00±0.00	0.01±0.00	0.01±0.00	0.01±0.00	0.01±0.00

For each TCA metabolite, data from glucose labeling is shown in the top row (not shaded) where those from glutamine labeling are shown at the bottom row (shaded). The percentage of labeling for each isotopomer is the fraction of that particular isotopomer over the total pool, including parent and various ^{13}C isotopomers. Data shown are the average and standard deviation from two independent experiments. Abbreviations: Glu, glutamate; αKG, α-ketoglutarate; Suc, succinate; Fum, fumarate; Mal, malate; Asp, aspartate; Cit, citrate.

Table S3. Transcriptional changes in ∆*KDH*/∆*IDH* double knockout parasite, related to Figure 2.

PlasmoDB ID	Gene Annotation	0h	6h	12h	18h	24h	30h	36h	42h	Avg Ratio
PF3D7_1149500	ring-infected erythrocyte surface antigen 2	3.76	2.55	1.70	1.15	0.59	0.29	1.20	1.36	1.57
PF3D7_1253000	DnaJ protein, putative	2.03	2.02	2.46	1.93	1.84	2.12	0.91	0.95	1.55
PF3D7_1201200	Plasmodium exported protein	2.18	1.80	1.61	1.38	0.91	0.53	1.21	1.56	1.40
PF3D7_1252900	Plasmodium exported protein	1.78	2.67	1.02	0.89	1.62	0.18	1.89	0.73	1.35
PF3D7_0530800	CPW-WPC family protein	0.14	0.71	2.08	0.93	2.36	1.81	1.92	0.25	1.27
PF3D7_1479000	acyl-CoA synthetase	2.28	2.04	0.11	1.30	0.87	0.43	1.43	1.59	1.26
PF3D7_0922300	conserved Plasmodium protein	1.13	0.75	1.25	0.48	1.53	0.87	1.67	1.47	1.14
PF3D7_0219900	Plasmodium exported protein	1.15	1.47	1.00	0.54	0.46	0.59	1.27	2.47	1.12
PF3D7_1449000	conserved Plasmodium protein	0.47	0.41	1.81	0.19	0.79	1.03	1.45	2.26	1.00
PF3D7_0424900	Plasmodium exported protein (PHISTa)	-2.20	-1.54	-2.55	-2.08	-1.38	-2.31	-2.00	-2.86	-2.11
PF3D7_0610400	histone H3	-2.41	-2.89	-2.12	-2.02	-1.66	-1.64	-2.06	-0.85	-1.96
PF3D7_0617800	histone H2A	-2.06	-2.38	-1.81	-1.65	-1.52	-1.70	-1.73	-1.10	-1.74
PF3D7_1016300	glycophorin binding protein	-1.18	-2.63	-1.46	-1.24	-1.21	-1.45	-2.45	-0.81	-1.55
PF3D7_1401500	lysophospholipase, putative	-1.74	-0.82	-1.44	-1.36	-1.31	-1.98	1.00	-1.74	-1.42
PF3D7_1418800	signal recognition particle, RNP	-3.56	-1.19	-0.55	-2.07	-1.01	-1.15	0.55	-2.20	-1.40
PF3D7_0814200	DNA/RNA-binding protein Alba	-0.61	-1.04	-0.36	-2.07	-1.64	-1.46	-1.85	-1.70	-1.34
PF3D7_1358800	40S ribosomal protein S13, putative	-1.19	-1.71	-0.99	-1.33	1.00	-0.56	-2.46	-1.20	-1.30
PF3D7_0201900	erythrocyte membrane protein 3	-1.32	-1.44	-0.89	-1.05	-1.40	-1.25	-0.80	-1.81	-1.24
PF3D7_1465900	40S ribosomal protein S3, putative	1.00	-1.71	-0.85	-0.90	-0.98	-1.10	-2.43	-0.94	-1.24
PF3D7_0520000	40S ribosomal protein S9, putative	-1.11	-1.49	-1.28	-0.90	-1.02	-0.49	-2.52	-0.98	-1.22
PF3D7_0930300	merozoite surface protein 1	-1.02	-1.54	-1.33	-2.12	-1.72	-0.69	-1.64	--0.5	-1.19
PF3D7_1453700	cochaperone p23	-0.99	-1.08	-0.32	-1.29	-1.18	-1.05	-1.96	-1.65	-1.19
PF3D7_1242700	40S ribosomal protein S17, putative	-0.89	-1.63	-0.97	-1.21	-1.08	-0.76	-2.15	-0.54	-1.15
PF3D7_0210100	60S ribosomal protein L37ae	-1.01	-1.50	-1.46	-0.92	-0.64	-0.80	-1.82	-0.61	-1.09
PF3D7_1105100	histone H2B	-1.37	-1.25	-1.26	-1.09	-0.73	-1.49	-1.15	-0.36	-1.09
PF3D7_0517000	60S ribosomal protein L12, putative	-0.84	-1.28	-0.87	-1.01	-0.96	-0.62	-2.07	-0.97	-1.08
PF3D7_0814000	60S ribosomal protein L13-2	-0.76	-1.35	-0.68	-1.05	-1.03	-0.74	-2.15	-0.74	-1.06
PF3D7_0616100	conserved Plasmodium protein	-1.16	-0.70	-0.02	-1.43	-0.96	-0.84	-0.74	-2.65	-1.06
PF3D7_0207600	serine repeat antigen 5	-1.06	-0.73	-0.65	-3.13	-0.71	-0.50	-1.27	-0.39	-1.05
PF3D7_1126200	40S ribosomal protein S18, putative	-1.15	-1.48	-0.67	-0.82	-0.52	-0.78	-2.21	-0.79	-1.05
PF3D7_1424100	60S ribosomal protein L5, putative	-0.62	-1.27	-0.93	-0.69	-0.93	-0.54	-2.35	-1.02	-1.04
PF3D7_0424800	Plasmodium exported protein (PHISTb), unknown function	-1.77	-1.04	-1.71	-0.61	-0.36	-0.65	-0.99	-1.16	-1.04
PF3D7_1309100	60S ribosomal protein L24, putative	-0.87	-1.24	-1.08	-1.29	-0.90	-0.82	-0.95	-1.11	-1.03
PF3D7_0415900	60S ribosomal protein L15, putative	-0.45	-1.16	-0.94	-0.80	-0.65	-1.05	-2.39	-0.80	-1.03
PF3D7_1426100	basic transcription factor 3b	-0.53	-1.47	-0.95	-0.89	-1.02	-0.50	-1.55	-1.25	-1.02
PF3D7_1317800	40S ribosomal protein S15/S19	-0.90	-1.15	-0.53	-1.02	-0.87	-0.55	-2.16	-0.97	-1.02
PF3D7_0730900	Plasmodium exported protein	-0.58	-0.90	-0.45	-0.41	-1.57	-1.26	-1.25	-1.61	-1.00

The table provides a list of genes showing significant alterations in transcription level in the ∆*KDH*/∆*IDH* double knockout line in comparison to D10 wildtype. Genes IDs, functional annotations and ratios of transcription level in ∆*KDH*/∆*IDH* over D10 at each time point are listed. Genes up-regulated in ∆*KDH*/∆*IDH* are shown in positive values whereas those down-regulated in the double knockout are shown in negative values.

Table S4. The ratios of +3 malate and +3 aspartate in TCA knockout lines labeled with U-^{13}C glucose, related to Figure 3.

	Δ*Aco*	Δ*KDH*	Δ*IDH*	Δ*KDH*/Δ*IDH*	Δ*SDH*
+3 malate	1.73±0.0.7	3.94±0.51	1.69±0.17	2.87±0.19	2.86±0.73
+3 aspartate	2.15±0.98	5.31±0.59	2.29±0.27	4.18±0.25	2.22±0.46

For each metabolite in each line, data were normalized to D10 wildtype and the ratios were averaged from 2-4 biological replicates. Data shown are averages ± standard errors.

Table S5. Mass spectrometry intensities for unlabeled and various isotopomers of each TCA metabolite in RBCs, D10 WT and 9 different TCA KO lines incubated with uniformly ^{13}C-labeled (U-^{13}C) glutamine, related to Figure 2.

In the Excel data sheet available online, column A indicates the TCA metabolites detected, including unlabeled ^{12}C compound and various ^{13}C compounds. Glu, glutamate; akg, α-ketoglutarate; suc, succinate; fum, fumarate; mal, malate; asp, aspartate; cit, citrate. Row 1 is the numeric order for all different samples. Row 2 indicates different samples, including RBC, D10 WT and 9 TCA KO lines.

Table S6. Mass spectrometry intensities for unlabeled and various isotopomers of each TCA metabolite in various TCA KO lines labeled with different ^{13}C compounds, related to Figures 3 and 4.

In the Excel data sheet available online, column A indicates the TCA metabolites detected, including unlabeled ^{12}C compound and various ^{13}C compounds. Abbreviations are the same as those in Table S5. In datasets MCL_1 and MCL_2, ΔAco line was labeled with U-^{13}C glutamine + 2-^{13}C glucose, U-^{13}C glucose, and U-^{13}C glutamine, individually. In datasets MCL_3 and MCL_4, ΔKDH line was labeled with U-^{13}C glucose and U-^{13}C glutamine, individually. In datasets MCL_5 to MCL_9, only U-^{13}C glucose labeling was carried out. In each dataset of MCL_1 to MCL_9, controls were D10 WT and RBC samples.

Supplementary Figure Legends

Figure S1. Schematic representation of the endogenous and the knockout genetic loci in TCA cycle genes, related to Figure 2. A model of double crossover recombination is shown in (A). Primers used for diagnostic PCR analyses in Figure S2 are shown in arrows. Restriction endonucleases used for Southern blot analyses in Figure S3 and the digestion patters are shown in each panel. Probes used for Southern blot analyses are depicted as bars. TCA cycle genes of *KDH-E1* (α-ketoglutarate dehydrogenase E1 subunit, PF3D7_0820700) (panel A), *SCS-α* (succinyl-CoA synthetase α subunit, PF3D7_1108500) (panel B), *SDH-Fp* (succinate dehydrogenase flavoprotein, PF3D7_1034400) (panel C), *CS* (citrate synthase, PF3D7_1022500) (panel D), *Aco* (aconitase, PF3D7_1342100) (panel E), and *IDH* (isocitrate dehydrogenase, PF3D7_1345700) (panel F) are knocked out. hDHFR, human dihydrofolate reductase; yDHODH, yeast dihydroorotate dehydrogenase.

Figure S2. Genetic confirmation of nine TCA knockouts, related to Figure 2. Southern blot analyses confirmed the genotypes of all nine TCA knockout lines in the D10 background. DNA samples from knockout lines and the D10 wildtype were digested with appropriate restriction enzymes (indicated at the bottom of each panel): Δ*KDH* (KpnI), Δ*SCS* (BglII), Δ*SDH* (HpaI), Δ*CS* (XbaI), Δ*Aco* (BsrGI) and Δ*IDH* (BsrGI). The diagnostic restriction digestion fragments were detected by specific ^{32}P-labeled probes. The sizes of fragments (kb) of each knockout and the D10 wildtype are shown. Genetic maps of wildtype and knockout lines are illustrated in Figure S1.

Figure S3. Glucose- and glutamine-derived carbon mix in the mitochondrion, related to Figures 2 and 3. The isotopic enrichment patterns of citrate were investigated in RBCs infected with (A) Δ*Aco* or (B) wildtype (D10) parasites incubated for 4 h in medium containing (i) U-^{13}C glutamine, (ii) U-^{13}C glucose, or (iii) U-^{13}C glutamine + 2-^{13}C glucose (a single ^{13}C in the second position of glucose). Please note the different scales for Δ*Aco* and D10 lines. The molecular structures of citrate isotopomers expected from various carbon sources are shown. Y-axes indicate the isotopic enrichment of each isotopomer in the total citrate pool. The mixed +5 citrate signal in (iii) shows that glutamine and glucose derived carbons are labeling the same citrate pool. Orange bars, U-^{13}C glutamine labeling; blue bars, U-^{13}C or 2-^{13}C glucose labeling; mixed bars, U-^{13}C glutamine

and 2-^{13}C glucose labeling; grey bars, other signal. Data shown are averaged results of three biological replicates.

Figure S4. Glucose utilization by the TCA cycle in knockout parasite lines, related to Figure 3. Simplified glycolysis and TCA pathways are shown on the top. Bar graphs show the percentage of isotopic enrichment (y-axes) of various ^{13}C TCA intermediates (x-axes) extracted from the D10 wildtype, Δ*KDH* and Δ*KDH*/Δ*IDH* parasite pellets. The molecular structures of the dominant ^{13}C intermediate corresponding to each column are shown. Carbons derived from glucose via *PEPC* reaction are depicted in blue, whereas those derived by pyruvate are shown in gold. Blue Xs indicate the enzymatic disruptions in each knockout line.

Figure S5. The effect of atovaquone on the TCA cycle, related to Figure 4. The D10 wildtype, *yDHOD* transgenic and Δ*KDH*/Δ*IDH* double knockout parasites were incubated for 4 h in U-^{13}C glucose medium, with and without 100 nM atovaquone. Isotopomers of TCA intermediates were analyzed. The intracellular metabolites extracted from various parasite lines were determined. (Top) A linearized depiction of TCA metabolism showing each of the expected isotopomers produced from U-^{13}C glucose labeling. Bar graphs represent the isotopic enrichment of each isotopomer observed in different parasite lines. Blue Xs indicate enzymatic disruptions; red Xs indicate enzymatic reactions inhibited by atovaquone.

Figure S6. The consequences of knocking out TCA enzymes on gametocytogenesis, related to Figure 5. (A) Growth curves of NF54 wildtype, NF54-Δ*KDH*, and NF54-Δ*Aco* parasites at asexual blood stage. (B) Representative Giemsa-stained images of parasite morphology in NF54 wildtype and NF54-Δ*KDH* parasite lines through the gametocyte stages I to V and exflagellation. EX, exflagellation. (C) Representative Giemsa-stained images of parasite morphology in NF54 wildtype and NF54-Δ*Aco* parasites on different days over the 20 day induction period. (D) Stage V gametocytemia of NF54 wildtype and NF54-Δ*Aco* parasites is shown from day 14 to day 20 post induction. Data shown is representative of 3 independent experiments. (E) The effect of 100 nM atovaquone on exflagellation in NF54 wildtype parasite. Mature gametocytes from the NF54 wildtype were incubated with atovaquone for 0.5, 2, and 24 h on days 16, 17, 18 post induction, respectively. Exflagellation percentage was determined as described in Experimental procedures. NF54 wildtype treated with atovaquone (black bars) and without atovaquone (blue bars).

Figure S1

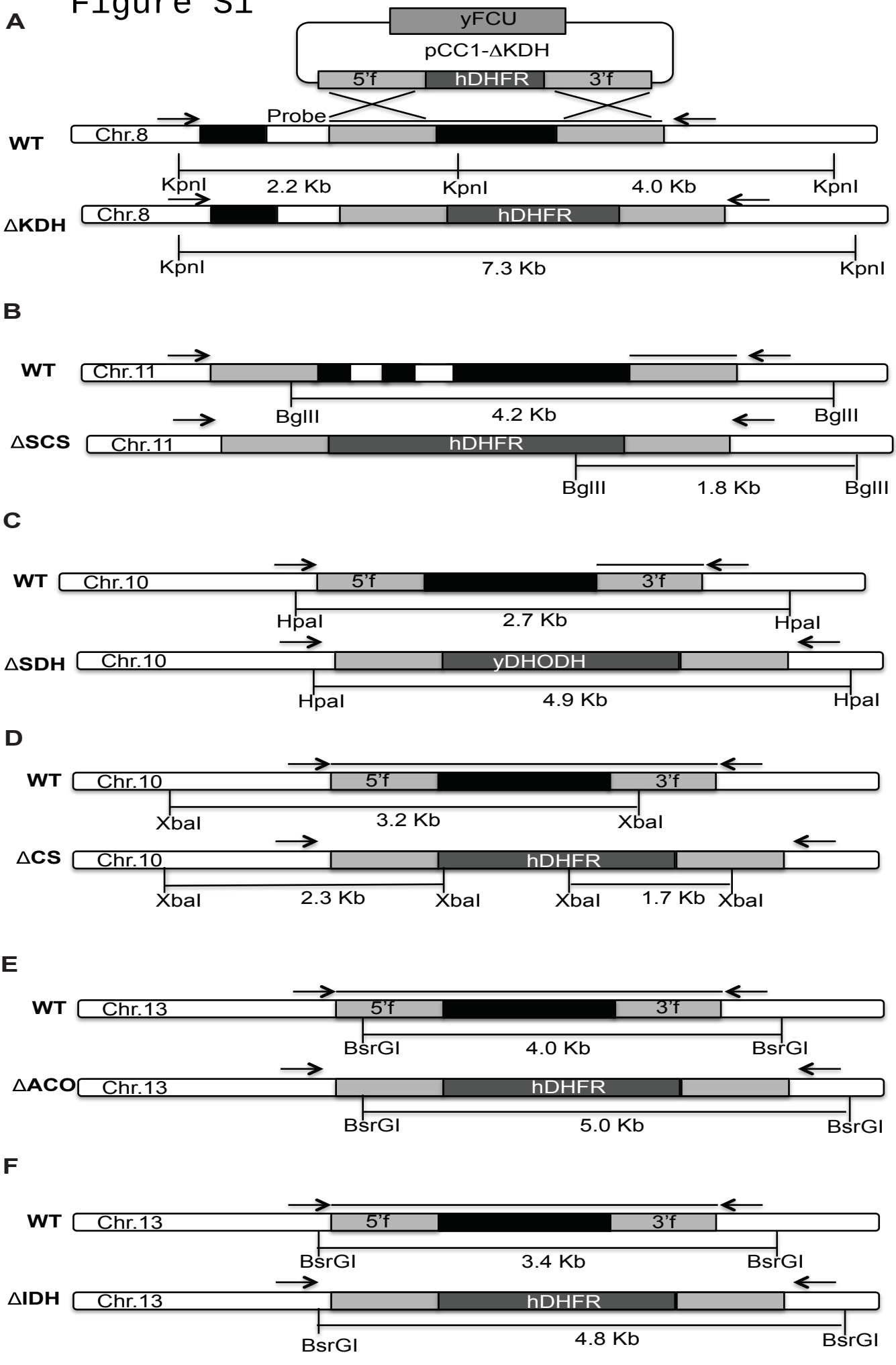
A
yFCU
pCC1-ΔKDH
5'f
hDHFR
3'f
Probe
WT
Chr.8
KpnI
2.2 Kb
KpnI
4.0 Kb
KpnI
ΔKDH
Chr.8
hDHFR
KpnI
7.3 Kb
KpnI
B
WT
Chr.11
BglII
4.2 Kb
BglII
ΔSCS
Chr.11
hDHFR
BglII
1.8 Kb
BglII
C
WT
Chr.10
5'f
3'f
HpaI
2.7 Kb
HpaI
ΔSDH
Chr.10
yDHODH
HpaI
4.9 Kb
HpaI
D
WT
Chr.10
5'f
3'f
XbaI
3.2 Kb
XbaI
ΔCS
Chr.10
hDHFR
XbaI
2.3 Kb
XbaI
XbaI
1.7 Kb
XbaI
E
WT
Chr.13
5'f
3'f
BsrGI
4.0 Kb
BsrGI
ΔACO
Chr.13
hDHFR
BsrGI
5.0 Kb
BsrGI
F
WT
Chr.13
5'f
3'f
BsrGI
3.4 Kb
BsrGI
ΔIDH
Chr.13
hDHFR
BsrGI
4.8 Kb
BsrGI

Figure S2

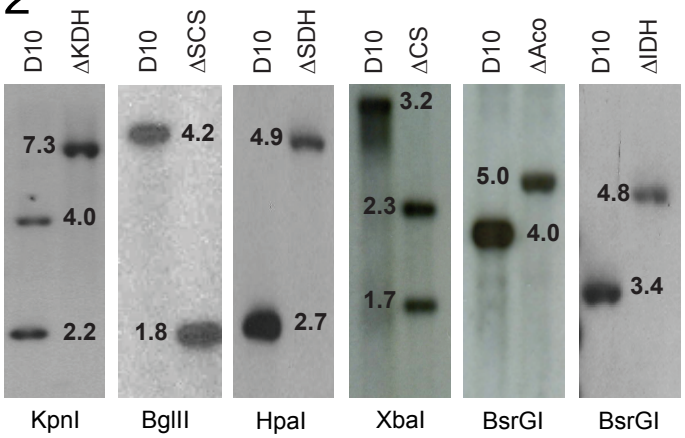
D10
ΔKDH
7.3
4.0
2.2
KpnI
D10
ΔSCS
4.2
1.8
BglII
D10
ΔSDH
4.9
2.7
HpaI
D10
ΔCS
3.2
2.3
1.7
XbaI
D10
ΔAco
5.0
4.0
BsrGI
D10
ΔIDH
4.8
3.4
BsrGI

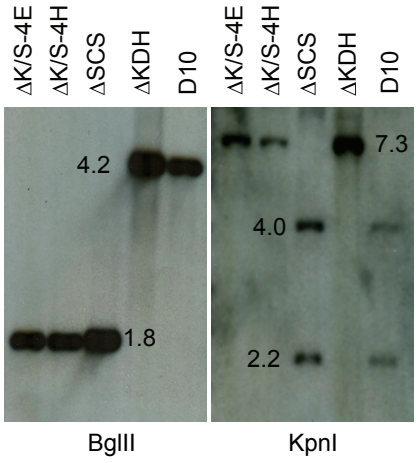
ΔK/S-4E
ΔK/S-4H
ΔSCS
ΔKDH
D10
4.2
1.8
BglII
ΔK/S-4E
ΔK/S-4H
ΔSCS
ΔKDH
D10
7.3
4.0
2.2
KpnI

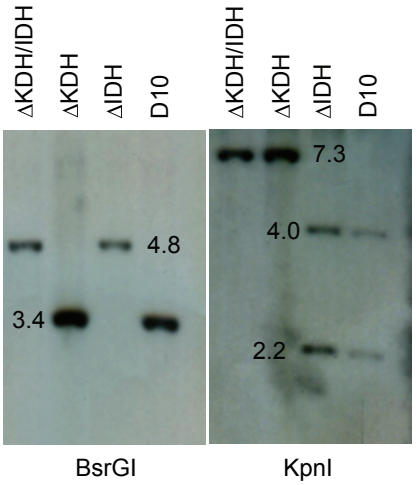
ΔKDH/IDH
ΔKDH
ΔIDH
D10
4.8
3.4
BsrGI
ΔKDH/IDH
ΔKDH
ΔIDH
D10
7.3
4.0
2.2
KpnI

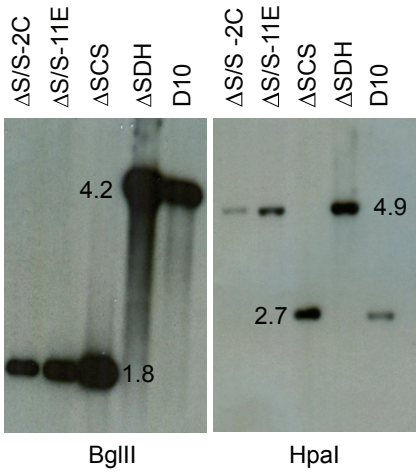
ΔS/S-2C
ΔS/S-11E
ΔSCS
ΔSDH
D10
4.2
1.8
BglII
ΔS/S -2C
ΔS/S-11E
ΔSCS
ΔSDH
D10
4.9
2.7
HpaI

Figure S3

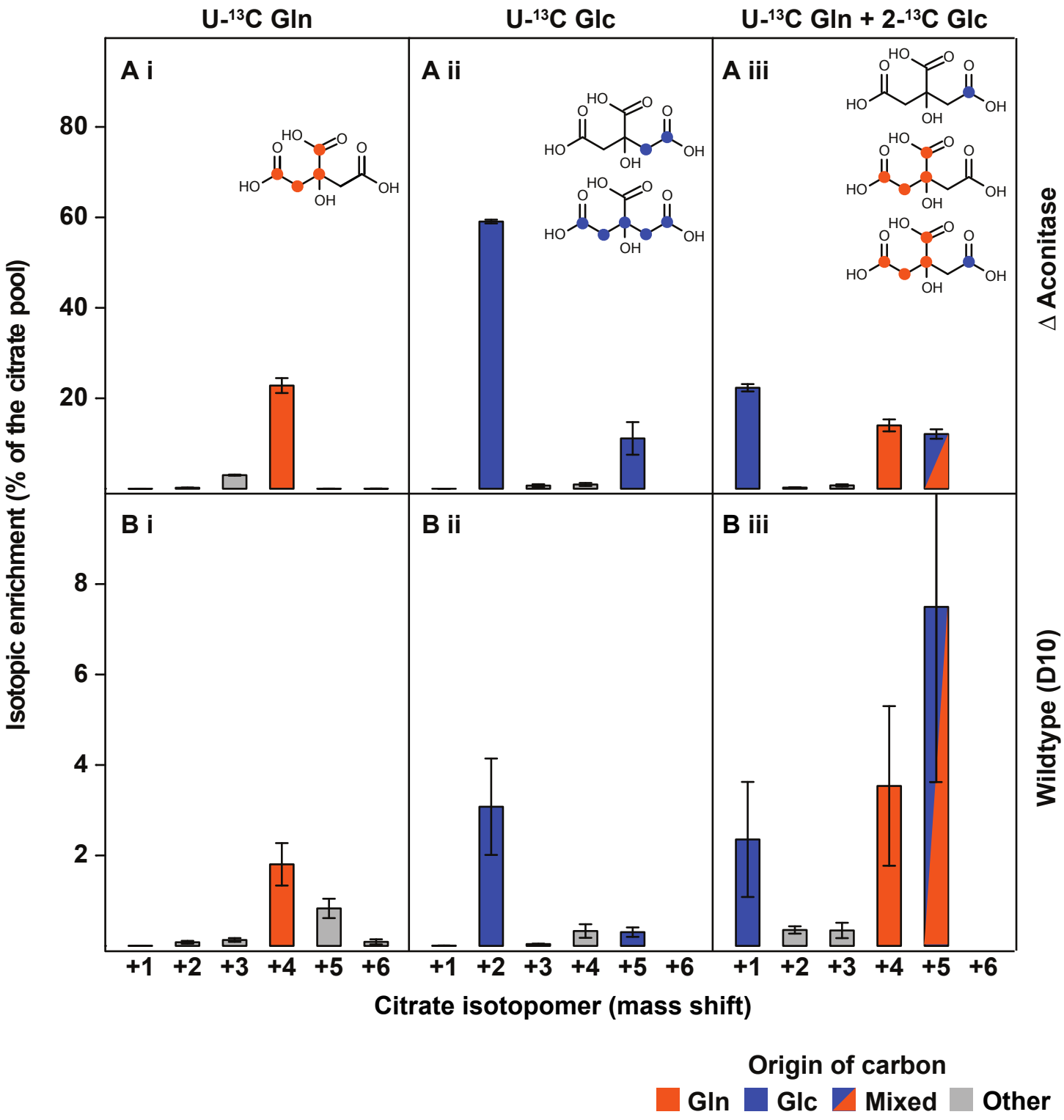
U-13C Gln
U-13C Glc
U-13C Gln + 2-13C Glc
A i
A ii
A iii
B i
B ii
B iii
Δ Aconitase
Wildtype (D10)
Isotopic enrichment (% of the citrate pool)
80
60
40
20
8
6
4
2
+1
+2
+3
+4
+5
+6
Citrate isotopomer (mass shift)
Origin of carbon
Gln
Glc
Mixed
Other

Figure S4

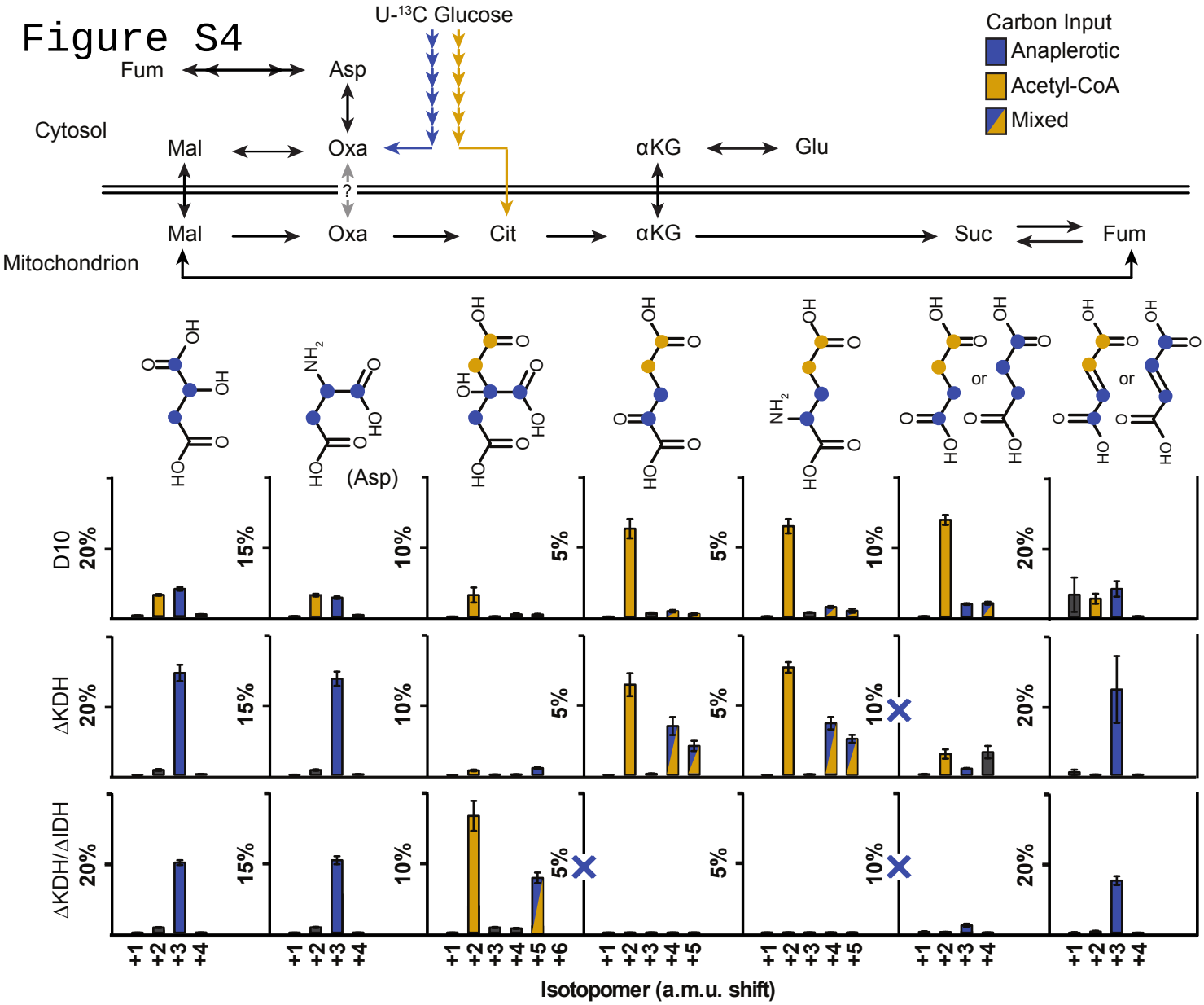
U-13C Glucose
Carbon Input
Anaplerotic
Acetyl-CoA
Mixed
Fum
Asp
Cytosol
Mal
Oxa
αKG
Glu
?
Mal
Oxa
Cit
αKG
Suc
Fum
Mitochondrion
(Asp)
or
or
D10
ΔKDH
ΔKDH/ΔIDH
20%
15%
10%
5%
+1 +2 +3 +4
+1 +2 +3 +4
+1 +2 +3 +4 +5 +6
+1 +2 +3 +4 +5
+1 +2 +3 +4 +5
+1 +2 +3 +4
+1 +2 +3 +4
Isotopomer (a.m.u. shift)

Figure S5

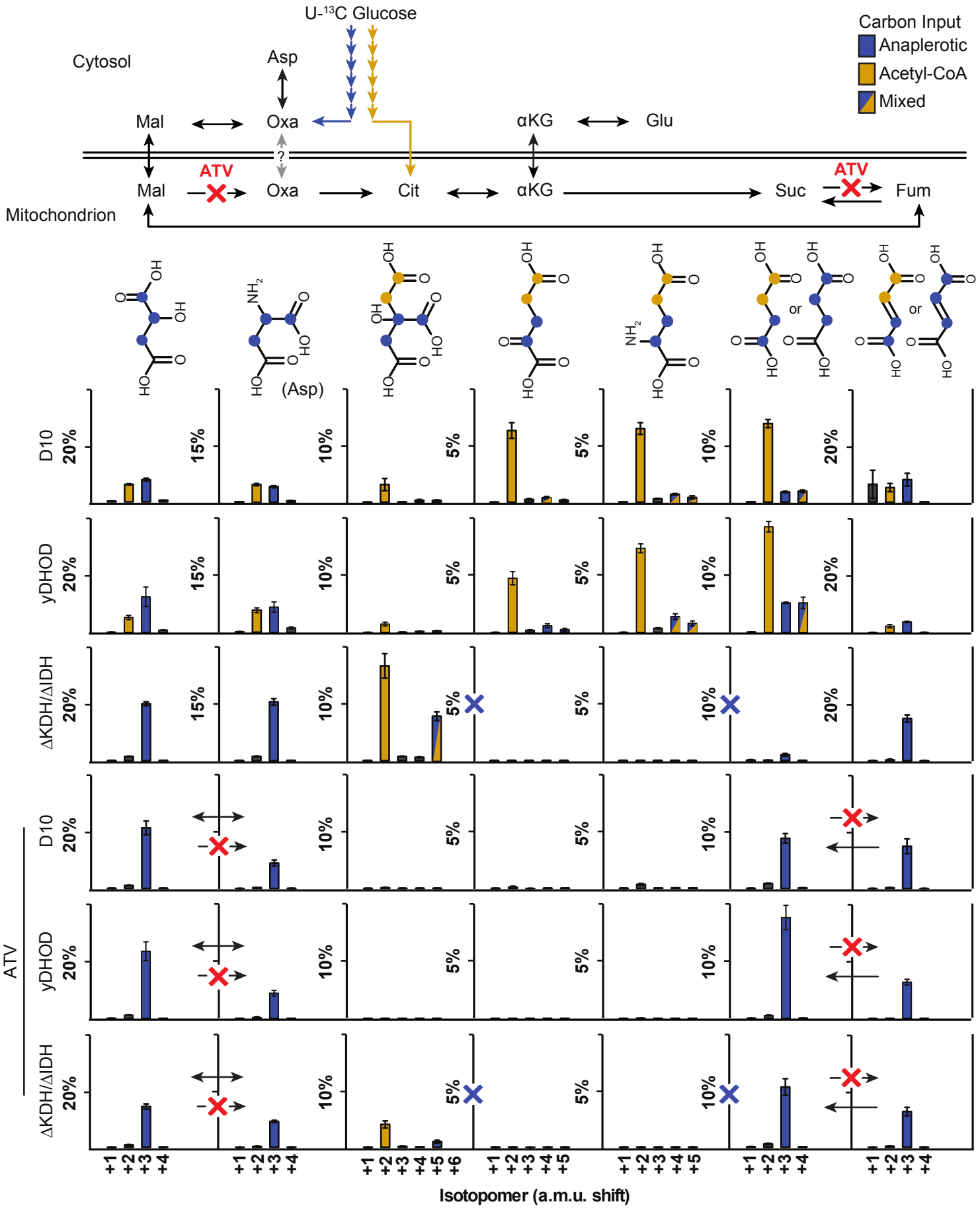
U-13C Glucose
Carbon Input
Anaplerotic
Acetyl-CoA
Mixed
Cytosol
Asp
Mal
Oxa
αKG
Glu
ATV
Cit
Suc
Fum
Mitochondrion
(Asp)
or
D10
yDHOD
ΔKDH/ΔIDH
ATV
Isotopomer (a.m.u. shift)

Figure S6

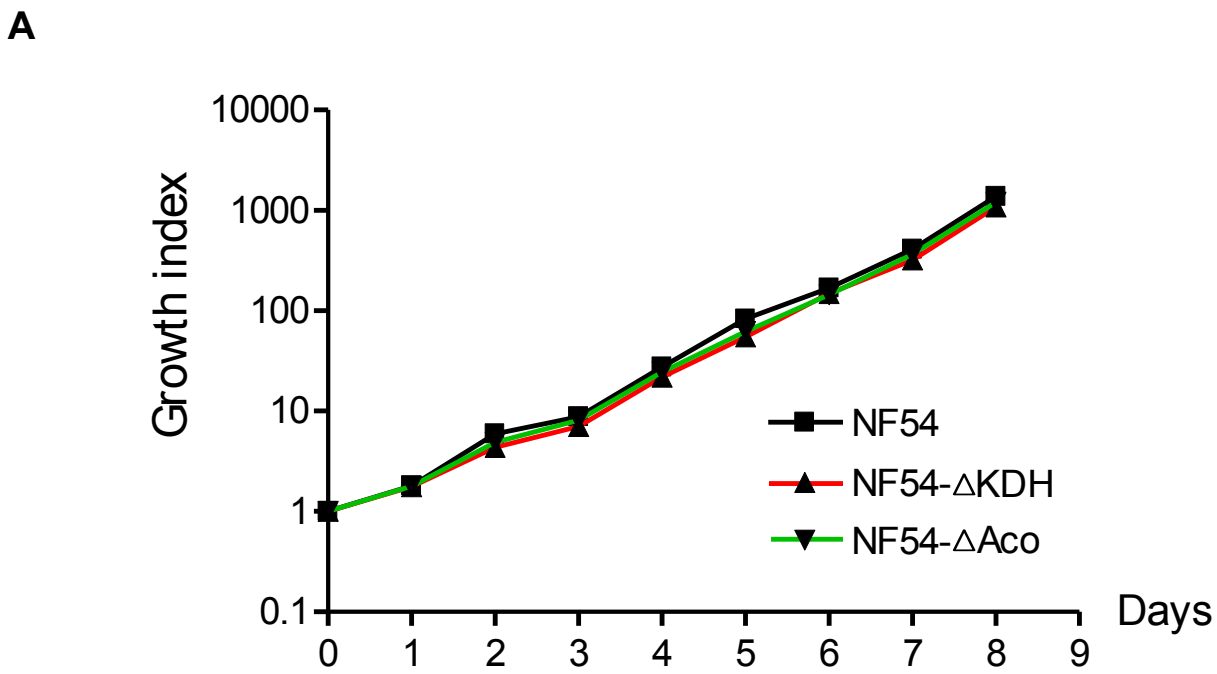
A
Growth index
10000
1000
100
10
1
0.1
0
1
2
3
4
5
6
7
8
9
Days
NF54
NF54-ΔKDH
NF54-ΔAco

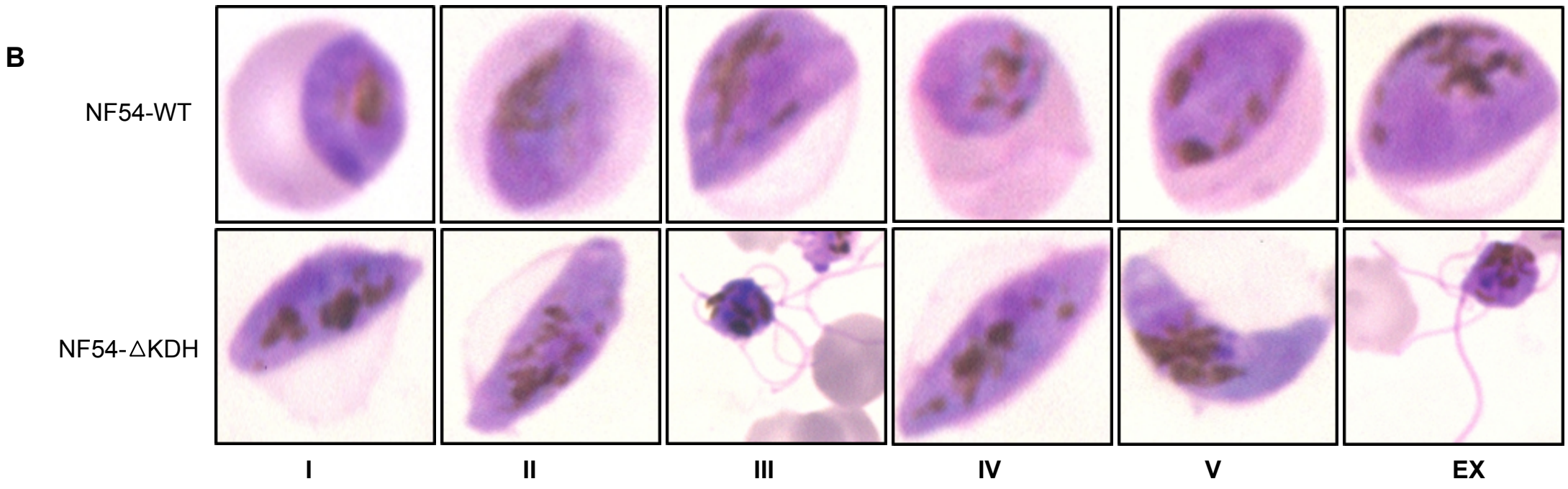
B
NF54-WT
NF54-ΔKDH
I
II
III
IV
V
EX

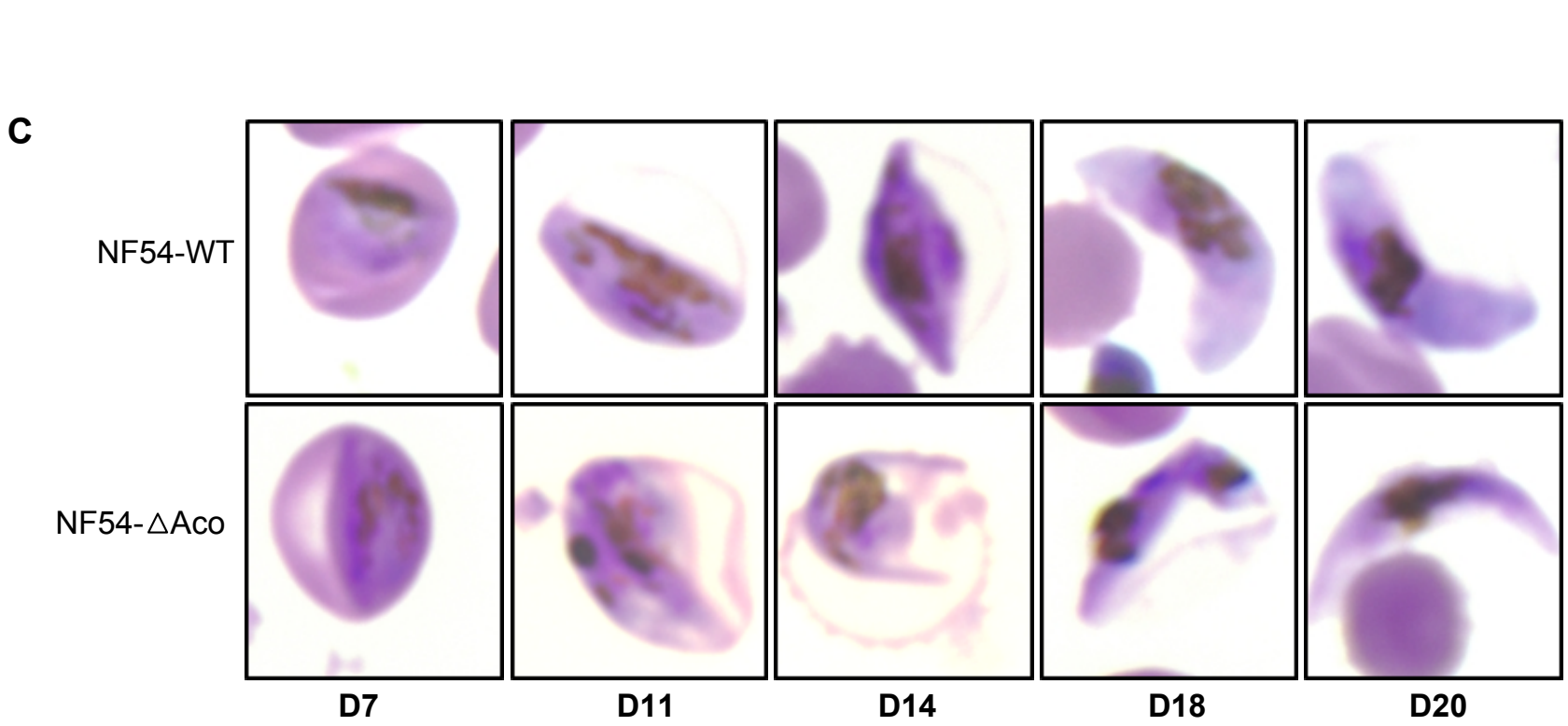
C
NF54-WT
NF54-ΔAco
D7
D11
D14
D18
D20

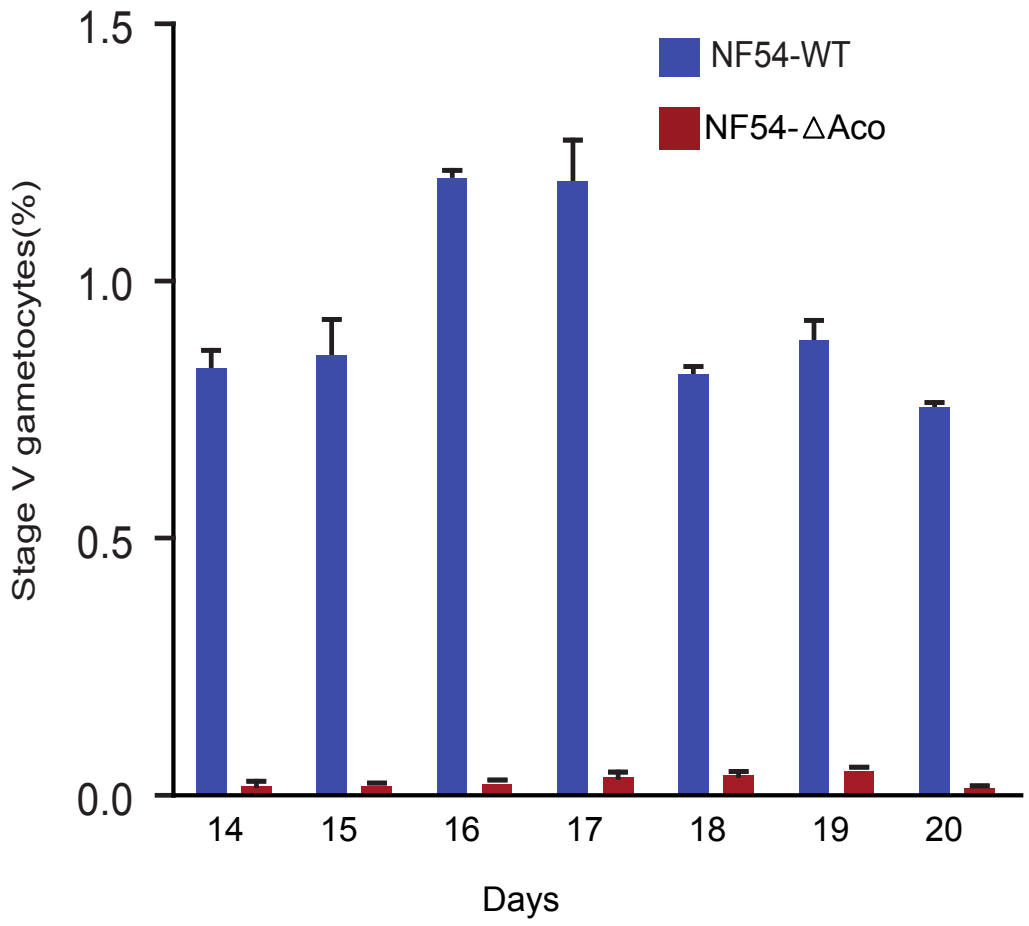
D
Stage V gametocytes(%)
1.5
1.0
0.5
0.0
14
15
16
17
18
19
20
Days
NF54-WT
NF54-ΔAco

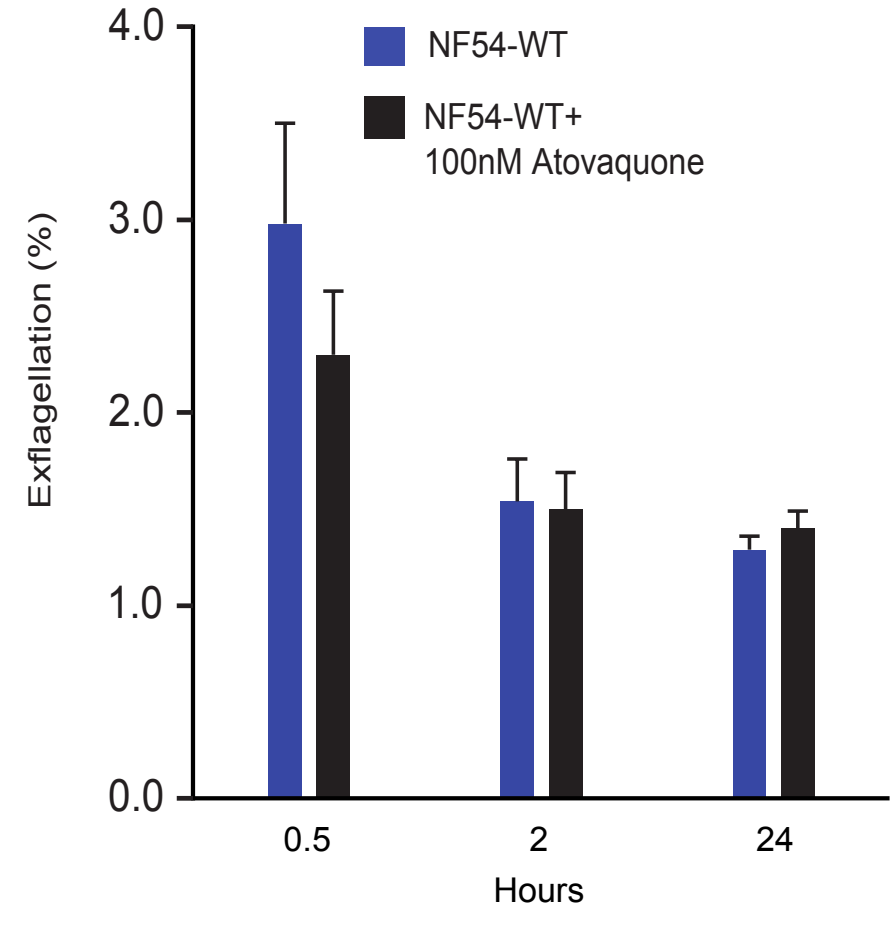
E
Exflagellation (%)
4.0
3.0
2.0
1.0
0.0
0.5
2
24
Hours
NF54-WT
NF54-WT+
100nM Atovaquone